Structure of the Paleoproterozoic Kédougou-Kéniéba Inlier (Senegal-Mali) deduced from gravity and aeromagnetic data

Mahamadou Diallo, Lenka Baratoux, Grégory Dufréchou, Mark Walter Jessell, Olivier Vanderhaeghe, Saïdou Ly, David Baratoux

Structure of the Paleoproterozoic Kédougou-Kéniéba Inlier (Senegal-Mali) deduced from gravity and aeromagnetic data.

Mahamadou Diallo[a,b], Lenka Baratoux[a], Grégory Dufréchou[a], Mark Walter Jessell[a,c], Olivier Vanderhaeghe[a], Saïdou Ly[b], David Baratoux[a]

[a] Géosciences Environnement Toulouse, IRD, UPS, CNRS 14 Avenue Edouard Belin, 31400 Toulouse, France
[b] Département de Géologie, Ecole Nationale d'Ingénieurs Abderhamane Baba Touré (ENI-ABT), 410, Av. Van Vollenhoven, BP 242, Bamako, Mali
[c] Centre for Exploration Targeting, The University of Western Australia, 35 Stirling Highway, Crawley, WA 6009, Australia

Corresponding author: M. Diallo: mahamadou.diallo@mesrs.ml

Abstract

The Kédougou-Kéniéba Inlier (KKI) corresponds to a window through Paleoproterozoic terranes of the West African Craton (WAC). This study presents, first of all, an interpretation of a regional Bouguer gravity map (14°W-9°W, 11°N-16°N) of the KKI and then introduces a new litho-structural map of the Malian part of the KKI using aeromagnetic data (12°0'W-10°80'W, 12°0'N-14°50'N). The KKI is limited to the west by a negative gravity anomaly forming a 30-100 km wide corridor, oriented N-S to NNE-SSW, and correlated to the Variscan Mauritanides orogenic belt. West of this belt, the Mesozoic to Cenozoic sedimentary deposits are marked by the highest positive anomaly of the region, attributed either to the presence of mafic rocks at intermediate to deep crustal levels or to a shallower Moho depth. Within the KKI, moderately positive to negative anomalies are correlated with exposed plutonic and mafic to intermediate metavolcanic rocks. Gravity data also reveal (i) two north-west trending lineaments attributed to crustal-scale shear zones, (ii) three north-east trending lineaments marked by gravity anomalies sub-parallel to the known Bissau–Kidira–Kayes Fault Zone, and named Kayes, Kédougou-Kéniéba, and South Shear Zones, respectively, (iii) and the extension to the south of the known Mauritanides Belt Thrust.

The local aeromagnetic map of the Malian part of the KKI discriminates the Mako metavolcanic belt with granitic intrusions in the west characterized by heterogeneous anomalies, from the Kofi metasedimentary series delineated by magnetic lows in the east. ESE-WNW to ENE-WSW-trending alternation of magnetic anomalies in the metavolcanic and metasedimentary rocks are attributed to pervasive structures associated with ductile

deformation. The Senegalo-Malian Shear Zone is marked at the regional scale by deflection of the geophysical lineaments but is not expressed by any offset of identified structures or lithological contacts.

Keywords: Airborne Magnetics; Gravity; Paleoproterozoic; West Africa; Mali; Structural Evolution

1. Introduction

Aeromagnetic and gravity data are a critical source of information for regional and local geology mapping and resource exploration, especially in zones of poor outcrop conditions owing to vegetation, soil and/or thick lateritic cover (*e.g.*, Hansen, 2001; Boyd and Isles, 2007). These data are useful at all stages of regional litho-structural mapping and mineral exploration programs. Gravity data provide an integrated response to density variations of rocks within the crust and down to the upper mantle, produced by structural and lithological contrasts at regional and local scales. This information is complementary to that obtained from aeromagnetic data, which provide better resolution of near surface when compared to gravity data. Together, these data can be used to identify lithological units, faults and their prolongation as major crustal shear zones (Gunn, 1997; Nabighian et al., 2005; Dufréchou et al., 2014; Aitken et al., 2016; Jessell et al., 2016). The structural features are defined as linear gravity or magnetic expressions caused by geological discontinuities at surface or at depth.
The structural geophysics approach (*e.g.,* Gunn et al., 1997; Crafford and Brauch, 2002; Boyd and Isles, 2007; Ranganai et al., 2008) utilizes the analysis of gravity and magnetic fields to interpret variations in mass and susceptibility that reflects the causative body characteristics. Transformations of potential field (gravity and magnetic) data enhance geophysical anomalies that are related to the observed field (Gunn, 1975). Interpretation of the geophysical anomalies offers the chance to explore, at the regional and local scale, the sub-surface distribution of geological properties (Gunn et al., 1997). Recognition of shear zones, deep-seated and second-order faults can be very important for mineral exploration, as these structures are widely regarded as the primary plumbing systems for migration of magmas and mineralizing fluids from the mantle or deep crust leading to deposit formation in the upper crust (*e.g.*, McCuaig and Kerrich, 1998; Crafford and Brauch, 2002; Dufréchou et al., 2015). Primary difficulties in gravity and magnetic data interpretation are to discriminate the

contribution to the geophysical field from sources located at different depths. It should be also noted that the interpretation of geophysical anomalies based on potential field data is intrinsically ambiguous as densities or susceptibilities are not uniquely related to rock type (*e.g.,* Emerson, 1990; Schön, 1996; Clark, 1997). Thereby, geological information becomes essential to constrain gravity and magnetic data interpretation.

This study focuses on the Kédougou-Kéniéba Inlier (KKI) and Kayes Inlier (KI), which comprises terranes affected by the Eburnean orogeny and overlain by Mesoproterozoic to Cenozoic sediments. These inliers are situated across southern Mauritania, eastern Senegal, northern Guinea and western Mali. Outcrop conditions are poor in the KKI/KI and crystalline basement rocks are widely masked by the lateritic cover and younger Quaternary deposits.

Previous studies have concentrated on geochemical, geochronological and structural analysis in the Senegalese part of the KKI (Bassot and Caen-Vachette, 1983; Bassot, 1987; Milési et al., 1989; Ledru et al., 1991; Dia et al., 1997; N'diaye et al., 1997; Gueye et al., 2007; 2008; Dabo and Aifa, 2010; 2011; Diene et al., 2012; 2015 and Diatta et al., 2017). Most of the Malian part of the KKI studies focused on mineralization at mining property-scale (Fouillac et al., 1993; Dommang et al., 1993; Lawrence et al., 2013a, b; Hein et al., 2015; Lambert-Smith et al., 2016a, b; Masurel et al., 2017a, b, c).

To complement the understanding of the Paleoproterozoic KKI and in order to fill gaps between sparse field observations, this paper presents an original analysis of gravity data at the regional scale and of the magnetic data at the scale of the Malian part of the KKI. These analyses are compared to published geological data in order to (i) place the KKI in its regional context, and (ii) decipher the main lithological units and structures of the KKI. The extension and internal structure of the KKI have been studied in detail with an emphasis on the structural framework and cross-cutting relationship between gravity and magnetic patterns related to regional tectonics. The shape and position of the lithology and structure of the KKI were better defined and several new major structures were identified and incorporated into the new interpretative map of the Malian part of the KKI.

2. Geological context and tectonic history of the KKI

2.1 Geological context

The regional gravity data analyzed in this study (Figs 1a and 2a) covers an area of 300,000 km² (14°W-9°W, 11°N-16°N) and straddles four countries: southern Mauritania, eastern Senegal, northern Guinea and western Mali. To the south, the Kenema-Man domain represents an Archean cratonic nucleus locally reworked during the Eburnean orogeny (Kouamelan et al., 1997). The Kédougou-Kéniéba Inlier (KKI) and Kayes Inlier (KI) correspond to windows through Mesoproterozoic to Neoproterozoic sediments of the intracratonic Taoudeni basin exposing the Paleoproterozoic basement. The KKI is bounded to the west by a polyphase mobile zone of the Variscan Mauritanides orogenic belt (Dia, 1988; Villeneuve, 2008) and from the south-east to north-east by the late Proterozoic to Paleozoic intracratonic Taoudeni basin (Fig. 2a).

The KKI is made of metavolcanic and metasedimentary rocks deformed and metamorphosed during the Eburnean orogeny (Bonhomme, 1962). It is subdivided into two metavolcanic belts (Mako and Falémé belts) and two metasedimentary series (Dialé-Daléma and Kofi series) (Bassot, 1987; Hirdes and Davis, 2002) (Fig. 1b). In the western part of the KKI, the NNE-SSW to N-S trending 20-40 km wide Mako belt (Fig. 1b) is characterized by a thick sequence of tholeiitic basalts, locally displaying pillow lavas, basaltic, gabbroic and ultramafic rocks of tholeiitic affinity as well as calc-alkaline basalts and andesites (Dia et al., 1997; Hirdes and Davis, 2002; Dioh et al., 2006; N'gom et al., 2009). The eastern margin of the Mako belt is in tectonic contact with the Dialé-Daléma series along the Main Transcurrent Zone (MTZ; Ledru et al., 1991). The Dialé-Daléma series is characterized by metasedimentary rocks with minor intercalations of metavolcanic rocks (Bassot, 1987; Dia, 1988; Hirdes and Davis, 2002; Gueye et al., 2008). It is intruded by several plutons, among these is the Saraya batholith (Pons et al., 1992) (Fig. 1b). The Falémé belt (Hirdes and Davis, 2002), east of the Dialé-Daléma series, consists of metapyroclastites, metarhyolites, metaandesites, minor metabasalts, metasedimentary rocks and syntectonic granitoids (Fig. 1b). The Kofi series is separated from the Faleme belt by the Senegalo-Malian Shear Zone (Bassot and Dommaget, 1986; Ledru et al., 1991; Lawrence, 2010). The Kofi series consists of detrital metasedimentary rocks, metacarbonate rocks and breccias (Lawrence et al., 2013a, Lambert-Smith, 2014; Masurel et al., 2017c) (Fig. 1b). It is intruded by monzodiorites, monzogranites and post-Paleoproterozoic mafic dykes (Baratoux et al., 2019).

2.2 Tectonic framework

The studied area covered by the gravity data, comprises the western edge of the West African Craton (WAC). It is cross-cut by the Mauritanides Belt Thrust to the west, and the Bissau–Kidira–Kayes Fault Zone (BKKF) in the north of the KKI, which cross-cuts the Mauritanides Belt (Villeneuve, 2008; Fig. 2a).

Three phases of deformation have affected the KKI during the Paleoproterozoic (Milési et al., 1989; Ledru et al., 1991; Dabo and Aïfa, 2011; Diene et al., 2012; Masurel et al., 2017a; Diatta et al., 2017). The D1 phase caused crustal thickening as a consequence of NE-SW to ENE-WSW horizontal shortening (Milési et al., 1989; Masurel et al., 2017c). The D1 phase is synchronous with the intrusion of large Tonalite-Trondhjemite-Granodiorite (TTG) batholiths within the Mako belt (Gueye et al., 2008; Diene et al., 2012). Contrariwise, Ledru et al. (1991) propose that the D1 has just affected the metasedimentary rocks of the Dialé-Daléma series and not those of the Mako belt. They infer an anteriority of the metasedimentary formations compared to the metavolcanic formations. However, the more recent geochronological data (Theveniaut et al., 2010) suggest that the Mako belt is older compared to the Dialé-Daléma series and therefore should have at least partially registered the D1 deformation event. The D2 phase is characterized by large N-S strike-slip faults and shear zones (Diene et al., 2012; Masurel et al., 2017c) and marks a change in tectonic style from collisional to transcurrent deformation (Dabo and Aifa, 2010; Diene et al., 2012). The D3 phase is characterized by the reactivation of early structures and the activation of ductile-brittle N-S to NE-SW trending sinistral shear zones accommodating NNW-SSE horizontal shortening (Diene et al., 2012; Lawrence et al., 2013b, Dabo et al., 2016; Masurel et al., 2017c). The Senegalo-Malian Shear Zone (SMSZ) is considered to be related to the D3 event (Bassot and Dommaget, 1986; Lawrence et al., 2013a), which consists of alternating low and high strain domains localized along lithological contacts between igneous and sedimentary rocks.

The subsidence of the large intra-cratonic Taoudeni basin forming a depression in the center of the WAC started in the Mesoproterozoic (Deynoux, 1971; Trompette, 1973) and continued until the mid-Paleozoic. The WAC was later deformed by the Pan-African and Hercynian orogenies as a consequence of a succession of collision and accretion events (Villeneuve et al., 1990).

3. Gravity data and interpretation

3.1 Gravity data sets and processing

The data from 3823 gravimetric stations were extracted from the Bureau Gravimétrique International (BGI) database (http://bgi.obs-mip.fr/) covering a larger area around the Malian part of the KKI (Fig. 1a and Fig. 2b). The gravimetric stations have variable spacing up to 6 km in the northern part of the studied zone and up to 20 km in its southern part (Fig. 2b). These gravity data were used to calculate a Bouguer gravity map with a 5 km cell size, over an area extending from 14°W to 9°W and from 11°N to 16°N (~542 km x 555 km). This area encompasses a region extending from southern Mauritania to northern Guinea and eastern Senegal to western Mali (Figs 1a and 2b).

The interpolation of gravity data was achieved using a minimum curvature algorithm (Briggs, 1974). Three sequential corrections, known as free-air, Bouguer and terrain correction have been made for the compensation of height and topographic effects. In this study, we have only applied the terrain correction as the free-air and Bouguer corrections were part of the BGI data-base. The terrain correction is the gravitational attraction, at the gravity station, of all the hills above the Bouguer slab and all the valleys occupied by the slab. It is obtained by determining the mass of the hills and the mass deficiencies of the valleys using topographic information. The topographic data used have an accuracy of 30m/pixel (Fig. 3b). The gravity measurement is influenced by the relief in the vicinity of a given measurement, in particular in the presence of rough topography. The terrain correction is made by calculating the regional terrain correction using a coarse regional Digital Elevation Model (at 90 m in our case) combined to a more finely sampled local DEM model covering the study area (at 30 m) (Fig. 3). The correction is applied to the entire Bouguer map, which includes both the flat Paleoproterozoic domain of the KKI and mountainous regions, such as the Meso to Neoproterozoic domains, including the Mauritanides Belt, the Northern Guinea and the Taoudeni Basin. The effect of the correction can be observed by comparing Figure 3a (before correction) and Figure 3c (after correction).

The process consists of creating a grid for the regional terrain correction (Fig. 3). We use in this process a crustal density value of 2.67 g.cm^{-3}, acknowledging that the resulting Bouguer anomaly is affected by this approximation (Flis et al., 1998). The grid is then used to calculate the detailed corrections at each gravity station with the appropriate module in the Geosoft Oasis Montaj software.

The obtained complete Bouguer anomaly map (Fig. 3c) provides information about mass distribution (variations in density) in the crust and in the upper mantle. As these density variations may be related to lithology, the Bouguer anomaly map allows for the identification of contacts between litho-tectonic domains (*e.g.*, Nabighian et al., 2005; Ranganai et al., 2008; Dufréchou and Harris, 2013; Dufréchou et al., 2014; Aitken et al., 2016). The first vertical derivative (1VD) and upward continuation (Fig. 4b and 4c) were calculated from gravity data in order to improve the definition of lithological boundaries and highlight deeper structures, respectively.

In order to determine the depth extent of structures mapped from the Bouguer gravity map and its first vertical derivative, multi-scale edge detection, called gravity worms (Archibald et al., 1999; Hornby et al., 1999; Holden et al., 2000; Horowitz et al., 2000) was produced (Fig. 5), using the Intrepid Geophysics software. This calculation is a wavelet transformation defining the positions of gradients at successive upward continued heights (Archibald et al., 1999; Holden et al., 2000). In this study, the gravity worm map (Fig. 5) was processed using seven steps of upward continuation from 7 to 58 km. The gravity worms represent discontinuities at all scales from local-scale shown by high-frequency features at lower levels of upward continuation to regional-scale, low-frequency features detected at higher levels of upward continuation. Dip direction can be inferred for sub-surface geological contacts (*e.g.*, lithological contact, faults and shear zones) based on the gravity worms map (Holden et al., 2000). Notably, the height levels of upward continuation may be related to the source depth. The upward continuation height is approximately twice the source depth of an idealized source geometry (*e.g.,* intrusions, faults, dykes) (*e.g.,* Archibald et al., 1999; Holden et al., 2000). Regional-scale structures are given names in the following text. Local-scale and near surface structures visible in the gravity worms map, which were not interpreted as regional-scale structures, were given numbers (Fig. 5) in order to refer to them in the following text.

3.2 Gravity patterns analysis: interpretation of regional geology

During the gravity data analysis, consideration was given to the KKI with the purpose to set its limit within the regional setting in relationship to its current surface extent. The Bouguer gravity anomalies range from about -30 to 50 mGal (Fig. 2b). The KKI is located between the Mauritanides Belt (Variscan Orogeny) to the west and the Neoproterozoic to Paleozoic Taoudeni basin to the east and south (Fig. 2). To the extreme west of the KKI, the Mesozoic-Cenozoic Senegalo-Mauritanian sedimentary basins (MCB; Fig. 2) are expressed by positive gravity anomalies (15 mGal to 51 mGal). This domain of positive anomalies extends further south and encompasses the Paleozoic sedimentary formations (Pa; Fig. 2b). The gravity worms (Fig. 5) mark well the eastern margin of the MCB along the contact with the Mauritanides Belt. Contiguous to the western side of the KKI, the fold-and-thrust Mauritanides Belt is characterized by positive gravity anomalies to the north (10 mGal to 35 mGal) and by pronounced negative gravity anomalies to the south (-4 mGal to –27 mGal). In the center and east of the studied area, the gravity anomalies are moderately positive (ca. 1 to 15 mGal) to negative (ca. -8 mGal to -27 mGal) and display a complex spatial pattern. This zone correlates with the Paleoproterozoic KKI and the Taoudeni Basin displaying similar gravity anomalies, which continue on both sides of the mapped KKI-Taoudeni boundary (KKI, KI, MNeP; Fig. 2b). This KKI-Taoudeni contact is no longer marked by any gravity lineament as seen in the gravity worms map (Fig. 5). The KKI-KI Paleoproterozoic metavolcanic/metasedimentary and plutonic rocks are associated either with positive or negative anomalies (10 mGal to -27 mGal; Fig. 2b). Commonly, the shape of a worm sheet in multiscale edge results from sharp discontinuities or interfaces between contrasting rock materials such as intrusive contact and highlights geological features (Holden et al. 2000). Indeed, a synthetic spherical worm sheet body is designed to represent a pluton intrusion type (Holden et al., 2000). A potential pluton at 15–20 km depth is inferred from an elongated rounded gravity worms (#1; Fig. 5b). This inferred intrusion is over a positive gravity anomaly suggesting a mafic intrusion elongated in a NNE-trending direction sub-parallel to the high level of the upward continuation of the West Mauritanides Thrust (WMT, Fig. 5b). Two previously undefined gravity worms features are depicted from gravity worms map (#2, #3; Fig. 5b). The worm #2 is marked by curved and large (up to 250 km) multi-scale edge detected all the way up to the 57 km upward continuation. The worm #2 shows a steep contact with a dip towards the NE in the south and towards the N in the north (#2; Fig. 5b). The worm #3 is a flat and curved SW-trending geological feature limited to the north by the KKSZ and to the south by the SSZ (#3; Fig. 4b). The gravity data (Figs 4b and 7c) shows several small regions with slightly negative gravity anomalies over the KKI corresponding to known granitic plutons (*e.g.*, Pons et al., 1992; N'diaye et al., 1997; Masurel et al., 2017c), such as Saraya, Gamaye, Moussala and Yatia (Ga, Mo, Yt; Fig. 7c). Several positive gravity anomalies up to ca. 10 mGal located in the KKI are correlated to mafic and ultramafic rocks (Fig. 7c).

The Mesoproterozoic to Neoproterozoic sedimentary units (MNeP) and associated plutons are characterized by contrasted gravity anomalies. The lithologies do not appear to be correlated with gravity anomalies in these units. These MNeP rocks occupy a large part of the analysed Bouguer map from the south to the east and northeast. Positive anomalies (1 mGal to 10 mGal) associated to the MNeP formations are interpreted as cropping out and buried mafic sills dated at 200 ± 3 Ma (Baratoux et al., 2019), while negative anomalies (-19 mGal to -27 mGal) are probably related to granitoid plutons and covering sediments (Fig. 2b). In summary, the studied area comprises two domains: (i) the western domain characterized by a positive gravity anomaly and (ii) the eastern domain characterized by heterogeneous patterns of positive and negative gravity anomalies.

3.3 Structural analysis from gravity data

The gravity data delineate straight or curved lineaments portrayed from (i) apparent alignment of gravity gradients; and (ii) offset of gravity anomalies across lineaments. These discontinuities are interpreted as an expression of faults and shear zones. The area comprises contrasted density domains affected by the Eburnean and Variscan Orogenies, and gravity data are expected to be useful in this context to reveal regional-scale faults and shear zones. The map of lineaments from gravity data proposed here must be considered as defining deep or broad deformation corridors rather than single and discrete faults at the surface.

Based on the gravity expression of the Mauritanides Belt Thrust (MbT) and the Bissau–Kidira–Kayes Fault Zone (BKKF), several new lineaments are identified from gravity maps (Fig. 4). The Mauritanides Belt Thrust may be extended to the south. A new sub-parallel lineament was drawn to the west of the southern part of the MbT, which is marked by a gravity lineament along the contact between contrasted gravity anomalies (positive gravity anomaly to the west and negative gravity anomaly to the east). This new structure, parallel to the MbT, corresponds to the southern continuation of mapped thrust zones that mark the western border of the MCB. We interpret this lineament as a thrust zone comparable to the MbT (WMT; Fig. 4 and Tab. 1) and name it the West Mauritanides Thrust (WMT). The WMT is well defined in gravity worms map (Fig. 5) where it sits at the contact between the MCB and the Mauritanides Belt. It is marked by a deep steep gravity worm discontinuity (Fig. 5).

Three new gravity lineaments, with characteristics similar to the Bissau–Kidira–Kayes Fault Zone (BKKFZ), are identified. These identified lineaments are considered as deep crust lineaments and are thereby interpreted as shear zones. The gravity lineaments sub-parallel to the BKKFZ are named the Kayes Shear Zone, the Kédougou-Kéniéba Shear Zone and the South Shear Zone (KSZ, KKSZ, SSZ; Figs 4, 5 and Tab. 1). The KSZ, in the north of the BKKF, marks a contact between a positive gravity anomaly in the south and a negative gravity anomaly in the north (KSZ; Fig. 4). The KSZ indicates a dip towards the SE, as shown by gravity worms (Fig. 5a). The KKSZ is associated with truncation of gravity anomalies and is the only gravity structure which cross-cuts the Malian Paleoproterozoic KKI (KKSZ; Figs 4 and 9). It is well defined in the first vertical derivative of the complete Bouguer gravity anomaly (Fig. 4b). The KKSZ marks the northern limit of a flat and curved SW dipping gravity worm (#3; Fig. 5b) as well as the northern limit of the long and steep, curved gravity worm (#2; Fig. 5b). The gravity worms indicate a steep dip towards the SE for the KKSZ. The

SSZ marks a contact between positive and negative gravity anomalies in its southern segment and shows truncation of positive gravity anomalies in its northern segment (SSZ; Fig. 4). In gravity worms, the southern part of the SSZ appears as the limit of the flat and curved SW dipping gravity worm (#3; Fig. 5b).

The analysis of gravity data allows the recognition of new NW-SE trending crustal-scale shear zones, which cross-cut the Mesoproterozoic to Neoproterozoic rocks and are visible in all gravity maps (Fig. 4). To the north of the studied area, the North Crustal Shear Zone (NCSZ) is characterized by contrasted gravity anomalies and by the truncation of gravity anomalies (NCSZ; Fig. 4 and Tab. 1). In gravity worms, the NCSZ is marked by the truncation and deflection of the worm (#2; Fig. 5a). To the south, a new gravity lineament sub-parallel to the NCSZ is portrayed and designated as the South Crustal Shear Zone (SCSZ; Fig. 4c and Tab. 1). The SCSZ is delineated by the truncation of positive gravity anomalies and by the contact between positive and negative gravity anomalies (SCSZ; Fig. 4). The SCSZ is only seen in gravity worms at its northern part as steep SW dipping structure (Fig. 5b). The upward continuation map to 20 km depth from the Bouguer gravity, provides information about deep regional-scale features (Fig. 4c). The gravity lineaments identified in the previous paragraphs (WMT, NCSZ, SCSZ, KSZ and SSZ, Fig. 4c) are also portrayed in the upward continued map (Fig. 3c). It should be noted that the KKSZ is less apparent; although it is confirmed by the worm #2 to be deep in its northern part (KKSZ; Fig. 4c).

The conjugate NE and NW-trending gravity worms (#4; Fig. 5b) are sub-parallel to the deep NCSZ and KKSZ structures, respectively. However, these gravity worms are near the surface as they are related to a low continuation value (< 25 km). The steep NE-trending gravity worms #5 and #6 do not correspond to any previously mapped structures. These lineaments (#5, #6; Fig. 5b) are considered as near-surface structures, as they are associated to a low continuation value (< 20 km). Both of these features have an indicated dip towards SE. The worm #6 passes through the Sadiola gold deposit and can be correlated to the deep expression of the NNE-trending thrust zone oblique to the Sadiola Shear Zone (Masurel et al., 2017a). The worm #7 is close to the deep NCSZ lineament (#7; Fig. 5b) and is interpreted to represent a regional gravity lineament that marks the southern limit of the steep and curved gravity worm #2 (#7; Fig. 5b). The worm #7 indicates a dip towards the NE. Three N-trending worms are portrayed from gravity worms map (#8, #9, #10; Fig. 5b). The worm #8 is steep with a dip towards the W and the worm #9 is less steep with a dip towards the W. The worm #10 is deeper than the worm #9 with a dip towards the W. The worms #8 and #9 are related to low continuation values (< 25 km), whilst the worm #10 is related to high continuation values (up to 50 km).

The Senegalo-Malian Shear Zone (SMSZ) and the Main Transcurrent Zone (MTZ) are regional shear zones described in the KKI (Bassot and Dommanget, 1986; Ledru et al., 1991) (Fig. 1b). They do not show evidence of truncation of gravity anomalies. However, the SMSZ marks the limit between the highly negative gravity anomaly of the Gamaye pluton (Ga; Fig. 7c) and the Falémé belt (K; Fig. 7c) in the south. The SMSZ seem to divide the F and G gravity anomalies (F, G; Fig. 7c) and to limit a few other gravity features as well (J; Fig. 7c).

4. Magnetic data

4.1 Magnetic data sets and processing

The aeromagnetic data used in this study (Figs 1b and 6) come from two main aeromagnetic surveys which were flown covering the Malian part of the KKI (High - Sense Geophysics/Aerodat Ltd, 1996, 1997; Kevron Pty Ltd, 2001). Their characteristics are summarized in Table 2.

Total Magnetic Intensity (TMI) data were reduced to the equator (RTE; Fig. 6a). The reduction to the pole (RTP) is less stable at the low magnetic latitudes than the reduction to the equator (RTE), which behaves well in low magnetic latitudes (Leu, 1982; Macleod et al., 1993). Several data transforms/derivatives were applied to the RTE in order to emphasize geological boundaries and major structures (Fig. 6).

The first vertical derivative (1VD; Fig. 6b) is used to delineate short wavelength features (Gunn et al., 1997; Milligan and Gunn, 1997). Thus, the 1VD map gives a sharper picture of the near-surface litho-structural features than the TMI (Verduzco et al., 2004) and was used to derive the structural framework of the studied area.

The absolute value of the analytic signal (AS; Fig. 6c) corresponds to the square root of the squared sum of the vertical and of the two horizontal derivatives of the magnetic field (Roest et al., 1992). The AS highlights the outlines of magnetic rock units and is effective for delineating geological boundaries. The AS resolves close-spaced bodies' relationship and is particularly useful for analyzing data from equatorial regions (McLeod et al., 1993).

The upward continuation transforms the data to attenuate near-surface features as if the measurements were made at a different height above the source (Milligan and Gunn, 1997) and highlight deeper structures masked by short wavelength anomalies (Jacobsen, 1987;

Lyngsie et al., 2006). The upward continuation is used to highlight magnetic and gravity anomalies (Figs 4c and 8b) associated with a pattern at 2.5 km and 20 km depth, respectively. The tilt derivative (Fig. 6d) is the arctangent of the ratio of the first vertical derivative and of the modulus of the total horizontal derivative (Miller and Singh 1994). For vertical magnetic bodies, the tilt derivative is positive over the source and negative outside of it. Because the tilt angle is based on a ratio, it responds well to both shallow and deep sources. The tilt images are used to trace the dolerite dyke swarm of the Malian part of the KKI (Fig. 9c).

4.2 Gravity and magnetic patterns: interpretation of the geology of the Malian KKI

The magnetic grain in the aeromagnetic data (Fig. 6) is interpreted to reflect deformed magnetic horizons. At the regional scale, these magnetic horizons correspond to three zones with distinct magnetic responses, which are correlated to the different litho-tectonic series forming the Malian part of the KKI (Figs 6 and 7b) (Hirdes and Davis, 2002; Villeneuve, 2008; Masurel et al., 2017c). The nomenclature used in this section refers only to the subdivision of magnetic signatures (Fig. 7b), namely, the west magnetic high (WMH), the east magnetic low (EML), the Finman magnetic signature (FP), the Taoudéni magnetic signature (Ta), and the south sill magnetic signature (Sd). The patterns of these magnetic domains and their response in gravity data, as shown in Figures 5 and 6c, are further discussed below.

The west magnetic high (WMH) encompasses the Mako belt (including the Finman pluton) and part of the Falémé belt and the Dialé-Daléma series. The east magnetic low (EML) corresponds to the Kofi series with internal dolerite sills (Sd; Fig. 6b). The Taoudeni magnetic signature (Ta) is related to Mesoproterozoic formation (Fig. 7b).

The Mako belt is characterized by heterogeneous magnetic signatures with ovoid to elongate high and low anomalies in the RTE image (Fig. 6a). Prominent sub-circular or ovoid-shaped lower magnetic anomalies of the analytic signal (A, C and D; Fig. 7a) correlate with granitic-dioritic plutons. Several pluri-kilometer-wide, elongate, and locally curved high anomalies are attributed to the presence of basaltic to andesitic rocks (E, F and H; Fig. 7a). The NNE-SSW ovoid-shaped moderately magnetic body in the center of the Mako belt corresponds to a calc-alkaline, amphibole-bearing pluton (C; Fig. 7a) dated at ca. 2140 Ma (Masurel et al., 2017c) and known as the Finman plutonic complex. It appears in the complete Bouguer anomaly map as negative anomalies without a defined form (C; Fig. 7c). In the AS map, a high magnetic anomaly is depicted in the WMH (F; Fig. 7a), which shows a circular shape in the RTE (F; Fig. 6a). This high magnetic anomaly F show a positive gravity anomaly in the Bouguer anomaly map (F; Fig. 7c). In gravity anomaly map, the F anomaly continues in the EML domains with a smooth texture (G; Fig. 7c). In the analytic signal map, the G anomaly (G, Fig. 7a) does not appear under the metasedimentary rocks of the Kofi series, but corresponds to the continuation of the F gravity anomaly under the Kofi series (F, G; Fig. 7a). The F and G anomalies are described as part of the Mako metavolcanic to meta-andesitic rocks.

The Dialé-Daléma series within the WMH is composed of clastic metasedimentary rocks with intercalated alkali pyroclastic flows (Bassot, 1987; Hirdes and Davis, 2002) (Fig. 1b), which are less magnetized than the Mako belt (Fig. 6a). The Dialé-Daléma series is characterized by a smooth magnetic texture with low magnetic anomalies. The series contains a folded high magnetic anomaly attributed to meta-andesites and meta-pyroclastic rocks (Mf; Figs 7a and 10). The Dialé-Daléma series is intruded in its Senegalese part by the Saraya granitoid complex (Sa; Fig. 7c; Pons et al., 1992), which shows large negative gravity anomaly in its northern side and positive gravity anomaly to its extreme southern side. The KKSZ marks the limit between the two gravity anomalies of the Saraya batholith (Fig. 7c). The northern extension of the Saraya batholith is known as the Moussala granodiorite (N'diaye et al., 1997) (Mo; Figs 6a and 7a, 7c). The Moussala granodiorite is well defined in gravity data with a prominent low anomaly. It has an elongated shape with a long axis trending NNE-SSW (Mo; Fig. 7c). The Moussala pluton is expressed by a low magnetic anomaly (Mo; Fig. 6a). The gravity data show at the eastern side of the Saraya batholith negative anomalies that are attributed to the presence of granitoids similar to the ones of the Saraya batholith beneath the Dialé-Daléma series (L; Fig. 7c).

The Falémé belt (J, K; Figs 6a and 7a) shows higher magnetization than the Dialé-Daléma series (Figs 1b and 7a), although its intensity and texture are variable. In the center-west of magnetic data (J; Fig. 6a), the Falémé belt presents high magnetic anomalies, which correspond to an orthogneiss cross-cut by an ESE-WNW trending mafic dyke (J; Fig. 7a). The southern portion of the Falémé belt expresses intermediate to high magnetic anomalies that are associated to diorite and amphibole granodiorite elongated in the N-S direction with calc-alkaline metavolcanoclastic rocks of the Boboti suite (Lambert-Smith et al., 2016b) (K; Fig. 7a). In gravity data, the (J) and (K) anomalies of Falémé belt are associated with positive gravity anomalies (J, K; Fig. 7c).

The east magnetic low (EML) of the analytic signal map corresponding to the Kofi series is marked by a low magnetic response with a smooth texture (Fig. 7b). The Kofi series is made of metasedimentary rocks alternating with calc-alkaline volcanic flows and pyroclastics (Fig. 1b; Masurel et al., 2017c). The metasedimentary components are weakly magnetized, and the igneous rocks give rise to moderate to high anomalies. The Yatia granite is the best example, which is marked by an ovoid-shape high magnetic anomaly with an E-W trending long axis (Yt; Fig. 6b and 7a) and a negative gravity anomaly (Yt; Fig. 7c). It is cross-cut by mafic dykes (Fig. 9a). In the south, the Gamaye granitic pluton (*e.g.*, N'diaye et al., 1997) does not appear in magnetic data and presents a textural appearance similar to the host metasedimentary rocks (Ga, Figs 6a and 7a). However, the Gamaye pluton is well-defined in gravity data with a negative gravity anomaly 40 km long and 15 km wide (Ga; Fig. 7c). A high amplitude magnetic anomaly is defined in the south of the Kofi series (Sd; Fig. 7a). This high magnetic anomaly corresponds to outcrops of NNE-SSW trending elongate doleritic sills (Sd; Fig. 7c).

The Mesoproterozoic cover of the Taoudeni basin (Ta) is associated with alternating high and low magnetic anomalies (Ta; Figs. 6 and 7). The sedimentary rocks correlate with low magnetic anomalies, and mafic sills correspond to high magnetic anomalies.

4.3 Structural analysis from magnetic data

The structural analysis is based on the first vertical derivative of the RTE map (Fig. 6b). The juxtaposition of sub-parallel and contrasting elongate magnetic horizons is categorized as lithological contacts or shear zones parallel to lithological units (Fig. 8 and Tab. 3). Long and deflected or dragged lineaments marking pronounced magnetic contrasts that can locally run parallel or cross-cut magnetic units on the enhanced derivative maps are interpreted as shear zones. Faults are characterized as straight and short offsets or abrupt truncations of magnetic horizons on the enhanced derivative maps.

4.3.1 Foliation, folds and shear zones

The lineament frequency depends on the magnetization of the analyzed domain and is higher in the metavolcanic rocks than in the metasedimentary rocks. This is especially the case of the metavolcanic Mako belt, which corresponds to the Western Magnetic High (WMH; Figs 7 and 8a). The most prominent lineaments are marked by alternating high and low anomalies interpreted to correspond to major magnetic lineaments. The metavolcanic Mako belt is characterized by generally high-strained, deflected and heterogeneously sheared magnetic units (Figs 6b and 8a). These magnetic features portray an early ductile deformation episode, with WNW-ESE to NW-SE trending direction. It is noteworthy that such structures have not been mentioned in previous work. The repetition of these lineaments and curved patterns of linear magnetic anomalies are attributed to isoclinal folds. This is well illustrated in the first vertical derivative map (Fig. 7b and Fig. 8a). In the entire West Magnetic High domain, folds display NW-SE, N-S, NE-SW and E-W axial traces (Fig. 8a and Tab. 3).

This early ductile fabric is cross-cut by N-S to NE-SW trending lineaments. The curvature of the WNW-ESE to NW-SE lineaments in the vicinity of the N-S to NE-SW trending lineaments suggests that the latter correspond to shear zones with an apparent dextral component (Tab. 3). These shear zones are regionally represented by the Main Transcurrent Zone (MTZ; Ledru et al., 1991) and the Senegalo-Malian Shear Zone (SMSZ; Basot and Dommanget, 1986). These later networks of ductile shear zones variably transposed the earlier deformation event with a regional reorientation of early lineaments from SW to NE and N within that frame. The MTZ is marked by a sharp and anastomosed network of lineaments cross-cutting E-W oriented magnetic units showing an apparent right-lateral offset of magnetic marker horizons (Fig. 8a and Tab. 3). The SMSZ corresponds to a N-S trending, long, and slightly curved lineament that follows the abrupt magnetic contact on the first vertical derivative map marking the limit between two contrasted magnetic domains (Fig. 8a and Tab. 3). The trace of the SMSZ marks the transition between a western domain characterized by the alternation of contrasted high and low magnetic anomalies associated with the Mako belt and Dialé-Daléma series and an eastern domain characterized by a more homogeneous magnetic signature corresponding to the Kofi series (Fig. 8b and Tab. 3). The WNW-ESE to NW-SE trending lineaments do not appear to be cross-cut by or dragged along the mapped trace of the SMSZ.

Comparing the metavolcanic belts of the Mako belt to the west and the metasedimentary rocks of the Kofi series to the east, we have shown that the aeromagnetic signatures of these two domains are different and none of the earliest E-W to WNW-ESE trending shear zones interpreted within the Mako belt are present within the Kofi series.

4.3.2 Faults

Several lineaments oriented ca. NW-SE to NNW–SSE, NNE–SSW to NE-SW, and E-W are identified from magnetic data and are interpreted as faults. They are marked by linear magnetic lows or highs or cross-cut and mark abrupt terminations of magnetic units (Fig. 8a and Tab. 3). The density of faults is variable throughout the studied area. They are related to bedrock structures as they show the intersection of metasediment units in the south of Kofi series (EML) and the truncation of meta-andesite and metavolcano-sedimentary rocks in the Mako belt (Tab. 3 ; Figs 8b and 10). The dominant faults in the Mako belt are NNE-SSW to

NE-SW trending, and they mainly show evidence of dextral movement. In contrast, the E-W interpreted fault in the Kofi series shows a dextral movement (Tab. 3; Fig. 10).

4.3.3 Dyke swarms

The tilt derivative highlights vertically dipping magnetic sources and is particularly useful to map dolerite dykes (Fig. 9a). Indeed, the tilt derivative map shows sublinear relatively narrow magnetic lows that delineate the two main groups of dyke swarms described in the KKI (Fig. 9b, 9c) (Théveniaut et al., 2010; Baratoux et al., 2019), namely (i) the 1764 ± 4 Ma Kédougou N035° trending dolerite dyke swarm; and (ii) the 1521 ± 3 Ma Sambarabougou N90° trending dolerite dyke swarm. These dykes, posterior to all Paleoproterozoic formations, are predominant in the Birimian domain (Jessell et al., 2015).

5. Discussion

5.1 Strengths and weaknesses of the different datasets

The integration of the available gravity and magnetic data with existing geological map (Fig. 1.b) proved to be useful for litho-structural mapping of the KKI (Fig. 10). As an example, illustrating the value of combining gravimetric and airborne magnetic data, the Gamaye granitic pluton does not appear in magnetics (Ga, Fig. 7a) but is well-defined in gravity data with a low gravity response of 40 km long and 15 km wide (Ga; Fig. 7c). Also, the dolerite sill in the south of Kofi series shows broad and well defined high magnetic anomaly (Sd, Fig. 7a, 7b); whilst, it does not show a gravity signature (Sd; Fig. 7c).

The variations in data resolution is a difficulty that may be turned into advantages to decipher the crustal structure when the data are analysed together in an integrated approach. Indeed, gravity data (Fig. 2b) is gridded at 5 km resolution (6 km spaced data points in the north and up to 20 km in the south) whereas the magnetic data (Fig. 6a) is gridded at 100 m resolution (200 m spaced lines). As a consequence, magnetic data is more suited for the near-surface as they capture better high-frequency features associated with near-surface structures and exposed lithologies (Fig. 10) and gravity is most useful to decipher deep structures, especially in the basement (Fig. 4).

Interpretations of correlations between geology and gravity remain locally uncertain. At some places, the gravity anomalies cannot be explained by surface geology. For instance, the highest density which is expressed as positive gravity anomaly over the sedimentary basins (Paleozoic to Mesozoic in age) in the western part of the analyzed extent of the gravity data (MCB; Fig. 2b) may reflect a large volume of dense material in the deep crust (mafic rocks) (*e.g.*, Gunn, 1997; Karner et al., 2005; Gao et al., 2017). This is inferred to compressed magma developed beneath the rifted area at the depocenters or edges of the Taoudeni sedimentary basin and/or may correspond to the uplifting of the Moho to the sub-surface giving high positive gravity anomalies over sedimentary basin. A strongly negative gravity anomaly is defined in the south of the Hercynian Mauritanides Belt, and this anomaly is difficult to understand considering the presence of mafic rocks (dense) at the surface (Villeneuve, 2008).

In summary, the detailed analysis of gravity and magnetic data, combined with geological information, has led to a revised litho-structural map of the Malian part of the KKI (Fig. 10) showing new or improved litho-structural information compared to the previously published map of the KKI (*e.g.*, Fig. 1b; Gueye et al., 2008; Lawrence et al., 2013a; Masurel et al., 2017c).

5.2 Litho-tectonic features interpreted from gravity and magnetic data analyses

The geophysical data presented in this paper compared to the known geology of the studied area provide new constraints on the lithological units and structures at the scale of the KKI and surrounding areas (gravity data) and at the scale of the Malian part of the KKI (combined gravity and magnetic datasets) (Figs 4, 8 and 9). This integrated approach of gravity and magnetic data confirmed previously recognized geological structures and led to several findings in the area of the Malian part of the KKI.

The Mauritanides Belt Thrust (MbT), as defined by geological data, is subdivided into three distinct segments. The north-western segment is marked by a limit between the highest density domain in the west and a high density domain in the east that corresponds to a positive gravity anomaly and coincides with the contact between the Senegalo-Mauritanian sedimentary basin and the Mauritanides Belt (MCB, Mb; Fig. 2). The north-eastern segment is not marked by a limit between contrasted gravity anomalies but is evidenced by offsets of negative gravity anomalies (Fig. 2b). The south-western segment is, however, not clearly delineated and cannot be traced in gravity maps.

The NE-SW trending Bissau–Kidira–Kayes Fault Zone (BKKF; Fig 2b) is well characterized in gravity data by the offset of the positive anomaly (10 mGal to 51 mGal) in its southern part where it shows truncation of the western domain. In its northern part, the BKKF marks the southern limit of the Kayes Inlier and the truncation of positive gravity anomaly (Fig. 3). The BKKF is not marked by any multi-scale edge detection in upward continued heights (Fig. 5a). Accordingly, the BKKF could be a sub-surface structure rather than a deep one. Other curved faults mapped by Villeneuve (2008) (Cf; Fig. 2a) do not correlate with gravity contrasts. The curved shapes of these faults from geological data suggest that they correspond to flat structures, which may not produce signatures in the gravity signal. The Bissau – Kidira – Kayes Fault zone permits interpretation of three other shear zones parallel to it, namely the Kayes Shear Zone, the Kédougou-Kéniéba Shear Zone and the South Shear Zone (KSZ, KKSZ and SSZ; Fig. 4). Only the KKSZ cross-cuts the magnetic data investigation area. The KKSZ runs through the Loulo district (Fig. 8) which is defined as world a class orogenic gold deposit (Dommanget et al., 1993; Lawrence et al., 2013a, b). However it is not expressed in magnetic data (Fig. 8) suggesting that this shear zone is a deep gravity lineament.

In Figures 7c and 8b, the pronounced gravity and magnetic patterns continue over the mapped KKI limit indicating a lateral continuation of the KKI greenstone belt under late Proterozoic to Paleozoic cover (Ta; Figs 7c and 8b) in the east. This is evidenced through the entire magnetic data from west to east as well as through gravity anomalies (F, G; Fig. 7c). On the other hand, the magnetic anomaly G does not appear in the RTE (Fig. 5a) as it is covered by magnetically quiet metasedimentary rocks, whilst this anomaly is well expressed in gravity data (G, Fig. 5c) and in the upward continued map (Fig. 8b). The occurrence of the KKI in this part of the WAC and its geophysical pattern continuation outside of its mapped limit suggests a continuity of the Paleoproterozoic basement underneath the sedimentary Taoudeni sequence from south to north. In contrast, the marked positive gravity anomaly to the west of the Mauritanides, interpreted as a step in the Moho, suggests that it represents the former western margin of the Paleoproterozoic KKI. These interpretations confirm previous models based on the interpretation of tomographic data (*e.g.,* Begg et al., 2009, Priestley et al., 2008, Jessell et al., 2016). In gravity map (Fig. 7c), the SMSZ and the MTZ are not characterized by gravity contrasts and thus may correspond to sub-surface structures or may mark a limit between contrasted geological domains as suggested from magnetic data.

Gravity data also highlight some lineaments that are not correlated to any identified surface structures yet. Two of these lineaments cross-cut the Paleoproterozoic KKI (SCSZ, KKSZ; Fig. 3) and only the KKSZ extends to the Malian part (Fig. 8a). Geological contacts exposed at the surface and magnetic horizons are not offset by these faults (Figs 4d and 8a). Most of the interpreted gravity lineaments are highlighted in gravity worms map (Fig. 4) and their depth, as well as their dip direction, were deduced from the upward continued gravity worms generated from continuation levels of 7.7 km to 57.7 km. These lineaments can be classified into two main groups: the NW-SE-trending lineaments and the NE-SW-trending lineaments. The movement along these lineaments cannot be inferred from the gravity data. However, from the gravity worms map, the worms #9 and #10 seem to be sinistrally offset along the SCSZ structure (Fig. 5). Accordingly, the SCSZ can be considered as a sinistral fault or shear zone as well the other NW-SE-trending lineaments, which are sub-parallel to the SCSZ. An important question is raised about the interpreted gravity lineaments origin. It is observed that these large structures do not offset the surface structures and stratigraphy. It is therefore speculated here that these lineaments are crustal-scale to lithospheric shear zones which might have formed before the final Paleoproterozoic assembly and could, therefore, correspond to earlier Eburnean or even pre-Eburnean structures or may have reactivated an Archean sub-crustal lineament (*e.g.,* Egal et al., 2002; Dufréchou and Harris, 2013; Dufréchou et al., 2014). Even though the origin of these lineaments is not defined, they could potentially have important implications for the structural and metallogenic evolution of the region (*e.g.,* Kohanpour et al., 2018), as the relationship between deep-seated gravity gradients and location of large deposits has been validated (Hobbs et al., 2000; Archibald et al., 2001; Dufréchou et al., 2011). In the gravity worms map, the gold deposits in the region occur in association with relatively shallow worms (#6, #7 and #8; Fig. 5). We note that these gravity worms are connected to the deepest worms in the study area (Fig. 5). These deep lineaments may potentially represent deep conduct through which, could offer connectivity from the mantle to the crust, and thus, characterize relatively shallow structural traps as shown by the gravity worms map (Fig. 5).

5.3 Implications for litho-tectonic evolution of the KKI

The previous tectonic model proposed for the KKI by Ledru et al. (1991) was based on the recognition of a polyphase structure for the Dialé-Daléma series with refolded folds that contrasts with the simple structure of the Mako belt characterized by a single NE-SW trending foliation. The polyphase structure of the Dialé-Daléma series is interpreted to record the succession of a D1 event followed by a D2 event, whereas the deformation of the Mako belt is ascribed to the D2 event. This proposition is contradicted by recent geochronological data in the KKI (Delor et al., 2010a, b; Théveniaut et al., 2010) dating magmatism of the Mako belt at ~2.2 Ga and deposition of the protolith of the metasedimentary formation of the Dialé-Daléma series after ca. 2165 Ma (Hirdes and Davis, 2002).

The gravity and magnetic lineaments provide new constraints for the reconstruction of the lithotectonic-evolution of the studied area, which updates and partly contradicts the model proposed by Ledru et al. (1991) but is coherent with the geochronological data obtained by Delor et al. (2010a, b) and Théveniaut et al. (2010). Indeed, magnetic data presented above show that the Mako belt, as the Dialé-Daléma series, are characterized by previously unrecognized WNW-ESE to NW-SE trending magnetic lineaments locally underlining isoclinal folds (Figs 6b and 8b). These lineaments are interpreted to represent an early phase of ductile deformation. Accordingly, we consider that the metavolcanic Mako belt has recorded the earliest increments of the local Paleoproterozoic tectonic event, as it is the case for the Dialé-Daléma series.

The lineaments attributed to this early D1 fabric are cross-cut by N-S to NE-SW trending lineaments, which we associate to transposition into D2 high-strain zones. The absence of E-W to WNW-ESE lineaments in the Kofi series, suggests either total transposition of the early fabric during D2 or that the protoliths of the Kofi series were deposited after D1. The transposition of E-W to WNW-ESE structures is particularly well expressed along the Main Transcurrent Zone (MTZ; Ledru et al., 1991) dominated by N-S to NE-SW lineaments (Fig. 8a and Tab. 3). However, the geometric relationships between E-W to WNW-ESE structures and N-S to NE-SW structures do not show large offset as in the case of a regional transcurrent displacement. The Senegalo-Malian Shear Zone (SMSZ; Basot and Dommanget, 1986) marks the boundary between a western magnetic domain characterized by highly contrasted magnetic anomalies and an eastern magnetic domain characterized by more homogeneous quiet magnetic signatures. The SMSZ is not associated with any horizontal offset of magnetic units and identified structures. Based on these considerations, we propose that the MTZ and SMSZ correspond to high-strain zones. The regional pattern of the Malian part of the KKI shows a reorientation of lineaments from the SW toward the N to NE, which either underlines the shape of former crustal blocks and/or suggests a strain gradient at this scale.

6. Conclusions

We have shown that the combination of gravity and magnetic data, leads to several significant findings complementing previously published work. The litho-tectonic map of the KKI was derived from this combination and new major structures were identified and incorporated in the Malian part of the KKI interpretative map (Fig. 10).

Gravity and magnetic analyses have shown that the KKI extends to the east underneath the Taoudeni basin but not to the west, where it is limited by the Mauritanides Belt. The eastward extension of the KKI was deduced from the continuation of anomalies with similar orientation and characteristics from both sides of the KKI-Taoudeni basin boundary.

Gravity anomaly map analysis led to several findings of new structures. The NW-trending North Crustal Shear Zone (NCSZ) and the South Crustal Shear Zone (SCSZ) are the most significant and are identified for the first time in the area. The Kédougou-Kéniéba Shear Zone (KKSZ), the Kayes Shear Zone (KSZ) and the South Shear Zone (SSZ) with NE-SW trend (Fig. 3) were also defined from gravity data (Fig. 4). The nature and significance of these structures have not been identified yet, but it should be mentioned that the Loulo with Gara and Yatea gold deposits (Figs 1b and 4) district is located close to the KKSZ.

Magnetic data covering the Malian KKI allow elaborating a new interpretative litho-structural map based on the geophysical features of the area (Fig. 10). Previously mapped ductile fabrics, shear zones, faults, dykes, felsic and mafic intrusions that were identified by geological mapping alone, are now extended, specified, and more precisely defined based on magnetic and gravity analysis. Mostly, three main generations of ductile structures are identified from magnetics with WNW-ESE to NW-SE, N-S to NNE-SSW and NE-SW and three fault trends with NW-SE, N-S to NE-SW and E-W. The earliest WNW-ESE to NW-SE lineaments-structures are transposed in the later N-S to NE-SW trending lineaments-structures. The analysis of magnetic data shows that the MTZ is characterized by sharp anastomosed magnetic lineaments cross-cutting early WNW-ESE to NW-SE lineaments without significant horizontal offset. Similarly, the SMSZ marks a limit between the contrasted magnetic domain of metavolcanic rocks and the quiet magnetic domain of metasedimentary rocks but does not show any horizontal offset of the magnetic units. These analyses of the MTZ and SMSZ question the importance of these shear zones as regional transcurrent tectonic structures.

Several NE-SW and E-W trending dolerite dykes cutting-across the KKI greenstone belt have been revealed, dated previously at ca. 1764 and 1520 Ma (Baratoux et al., 2019). The directions of these sparsely outcropping dolerite dykes have been deducted from this study. Therefore, the concomitance of dyke direction with fault and shear directions in the KKI (Fig. 9), highlighted from magnetic dyke mapping, suggests that the mafic magmas follow pre-existing zones of weakness.

This study illustrates the value of undertaking a combined analysis of gravity and magnetic data for litho-structural mapping.

Acknowledgements

This paper is a part of a PhD study financed by the French Ministry of Research through SCAC/Mali and by the WAXI project. This PhD program is run under a co-tutelle agreement between Université de Toulouse III (France) and Ecole Nationale d'Ingénieurs Abderhamane Baba Touré (ENI-ABT; Bamako, Mali). We wish to gratefully acknowledge AMIRA

International and the industry sponsors, for their support of the WAXI project (P934A). This research also received financial support from the program NEEDS (Nuclear, Energy, Environment, Waste and Society) "Multi- scale spatial distribution of U-Th: geostatistical studies from the mineral to the crust". Finally, the authors sincerely thank the anonymous reviewers for their thoughtful and careful comments on this manuscript.

References

Aitken, A.R.A., Betts, P.G., Young, D.A., Blankenship, D.D., Roberts, J.L., Siegert, M.J. 2016. The Australo-Antarctic Columbia to Gondwana transition. *Gondwana Research* 29 (2016) 136–152.

Archibald, N., Gow, P., Boschetti, F., 1999. Multiscale edge analysis of potential field data. *Exploration Geophysics* 30 (2): 38–44.

Baratoux, L., Soderlund, U., Ernst, R.E., de Roever, E., Jessell, M.W., Kamo, S., Naba, S., Perrouty, S., Metelka, V., Yatte, D., Grenholm, M., Diallo, D.P., Ndiaye, P.M., Dioh, E., Cournède, C., Benoit, M., Baratoux, D., Youbi, N., Rousse, S., Bendaoud, A. 2019. New U-Pb baddeleyite ages of mafic dyke swarms of the West African and Amazonian Cratons: implication for their configuration in supercontinents through time. In: Srivastava, R.K., Ernst, R.E., Peng, P. (eds.) (2019) Dyke Swarms of the World – A Modern Perspective. *Springer book volume*. Doi: 10.1007/978-981-13-1666-1_7.

Bassot, J. P. 1987. Le complexe volcano-plutonique calco-alcali de la riviere dalema (Est Senegal): discussion de sa signification geodynamique dans le cadre de l'orogenie eburneenne (proterozoique inferieur). *Journal of African Earth Sciences (1983)* 6 (4): 505–519.

Bassot, J. P., and Caen-Vachette, M., 1983. Donneés nouveles sur l'age du massif de granitoide du Niokolo-Koba (Sénégal Oriental); implication sur l'age du stade precoce de la Chaine des Mauritanides. *Journal of African Earth Sciences (1983)* 1 (2): 159–165.

Bassot, J.-P., and A. Dommanget. 1986. Mise en évidence d'un accident majeur affectant le Protérozoïque inférieur des confins sénégalo-maliens. *Comptes rendus de l'Académie des sciences. Série 2, Mécanique, Physique, Chimie, Sciences de l'univers, Sciences de la Terre* 302 (17): 1101–1106.

Begg, G. C., W. L. Griffin, L. M. Natapov, Suzanne Y. O'Reilly, S. P. Grand, C. J. O'Neill, J. M. A. Hronsky, Y. Poudjom Djomani, C. J. Swain, and T. Deen. 2009. The lithospheric architecture of Africa: Seismic tomography, mantle petrology, and tectonic evolution. *Geosphere* 5 (1): 23–50.

Boher, M., Abouchami, W., Michard, A., Albarede, F., and Arndt, N. T. 1992. Crustal growth in West Africa at 2.1 Ga. *Journal of Geophysical Research: Solid Earth* 97 (B1): 345–369.

Bonhomme, M. 1962. Contribution à l'étude géochronologique de la plate-forme de l'Ouest africain. *Imprimerie Louis-Jean*.

Boyd, D. M., Isles, D. J., 2007. Geological Interpretation of Airborne Magnetic Surveys - 40 Years On. In "Proceedings of Exploration 07: Fifth Decennial International Conference on *Mineral Exploration*" edited by B. Milkereit, 2007, p. 491-505.

Briggs, I. C. 1974. Machine contouring using minimum curvature. *Geophysics* 39 (1): 39–48.

Crafford, A. E. J., and V. J. S. Grauch. 2002. Geologic and geophysical evidence for the influence of deep crustal structures on Paleozoic tectonics and the alignment of world-class gold deposits, north-central Nevada, USA. *Ore Geology Reviews* 21 (3-4): 157–184.

Dabo, M., and Aifa, T. 2010. Structural styles and tectonic evolution of the Kolia-Boboti sedimentary basin, Kédougou-Kéniéba inlier, eastern Senegal. *Comptes Rendus Geoscience* 342 (10): 796–805.

Dabo, M., and Aïfa, T. 2011. Late eburnean deformation in the Kolia-Boboti sedimentary basin, Kédougou-Kéniéba inlier, Senegal. *Journal of African Earth Sciences* 60 (3): 106–116.

Dabo, M., Aïfa, T., Miyouna, T., Diallo, D.A., 2016. Gold mineralization paragenesis to tectonic structures in the Birimian of the eastern Dialé-Daléma Supergroup, Kédougou-Kénieba inlier, Senegal, West African Craton. *International Geology Review* 58, 807– 825.

Delor, C., Couëffé, R., Goujou, J.-C., Diallo, D.P., Théveniaut, H., Fullgraf, T., Ndiaye, P.M., Dioh, E., Barry, T.M.M., Le Métour, J., Martelet, G., 2010a. Carte géologique à 1/200,000 du Notice explicative de la carte géologique à 1/200,000 du Sénégal, feuille Tambacounda-Dalafi Ouest- 76-Sénégal, feuille Saraya – Kédougou Est. Ministère des Mines, de l'Industrie, de l'Agro-Industrie et des PME, Direction des Mines et de la Géologie, Dakar.

Delor, C., Couëffé, R., Goujou, J.-C., Diallo, D.P., Théveniaut, H., Fullgraf, T., Ndiaye, P.M., Dioh, E., Blein O., Barry, T.M.M., Cocherie, A., Le Métour, J., Martelet, G., Sergeev, S., Wemmer, K., 2010b. Notice explicative de la carte géologique à 1/ 200,000 du Sénégal, feuille Saraya – Kédougou Est. Ministère des Mines, de l'Industrie, de l'Agro-Industrie et des PME, Direction des Mines et de la Géologie, Dakar.

Deynoux, M., and Université d'Aix-Marseille 3 Laboratoire de géologie dynamique. 1971. Essai de synthèse stratigraphique du bassin de Taoudéni (Précambrien supérieur et Paléozoïque d'Afrique occidentale). Saint-Jérôme, Laboratoires des sciences de la terre, Faculté des sciences.

Dia, A. 1988. Caractéres et signification des complexes magmatiques et métamorphiques du secteur de Sandikounda-Laminia (Nord de la boutonnière de Kédougou, Est du Sénégal): un modèle géodynamique du Birimien de l'Afrique de l'Ouest. *Ph. D. thesis*, 350 pages.

Dia, A., Van Schmus, W.R. Kröner, A., 1997. Isotopic constraints on the age and formation of a Palaeoproterozoic volcanic arc complex in the Kédougou inlier, eastern Senegal, West Africa. *Journal of African Earth Sciences*, 24: 197-213.

Diatta, F., Ndiaye, P.M., Diène, M., Amponsah, P.O., Ganne, J. 2017. The structural evolution of the Dialé-Daléma basin, Kédougou-Kéniéba Inlier, eastern Senegal. *Journal of African Earth Sciences* 129: 923–933.

Diene, M., Gueye, M., Diallo, D.P., Dia, A. 2012. Structural evolution of a Precambrian segment: Example of the Paleoproterozoic formations of the Mako belt (eastern Senegal, West Africa). *International Journal of Geosciences* 3 (01): 153.

Diene, M., Fullgraf, T., Diatta, F., Gloaguen, E., Gueye, M., Ndiaye, P.M., 2015. Review of the Senegalo-Malian shear zone system – Timing, kinematics and implications for possible Au mineralisation styles. J. Afr. Earth Sci., http://dx.doi.org/10.1016/j.jafrearsci.2015.05.004

Dioh, E., Béziat, D., Debat, P., Grégoire, M., Ngom, P.M. 2006. Diversity of the Palaeoproterozoic granitoids of the Kédougou inlier (eastern Senegal): Petrographical and geochemical constraints. *Journal of African Earth Sciences* 44 (3): 351–371.

Dufréchou, G., Harris, L.B., Corriveau, L., Antonoff, V., 2011. Gravity evidence for a mafic intrusion beneath a mineralized zone in the Bondy gneiss complex,Grenville Province, Quebec – Exploration implications. *Journal of Applied Geophysics* 75, 62–76.

Dufréchou, G., and Harris, L.B. 2013. Tectonic models for the origin of regional transverse structures in the Grenville Province of SW Quebec interpreted from regional gravity. *Journal of Geodynamics* 64: 15–39.

Dufréchou, G., Harris, L.B., Corriveau, L. 2014. Tectonic reactivation of transverse basement structures in the Grenville orogen of SW Quebec, Canada: insights from gravity and aeromagnetic data. *Precambrian Research* 241: 61–84.

Dufréchou, G., Harris, L.B., Corriveau, L., Antonoff, V. 2015. Regional and local controls on mineralization and pluton emplacement in the Bondy gneiss complex, Grenville Province, Canada interpreted from aeromagnetic and gravity data. *Journal of Applied Geophysics* 116: 192–205.

Egal, E., Thiéblemont, D., Lahondere, D., Guerrot, C., Costea, C. A., Iliescu, D., Delor, C., Goujou, J.C., Lafon, J.M., Tegyey, M. 2002. Late Eburnean granitization and tectonics along the western and northwestern margin of the Archean Kénéma–Man domain (Guinea, West African Craton). *Precambrian Research* 117 (1-2): 57–84.

Flis, M. F., Butt, A. L. Hawke, P. J., 1998. Mapping the range front with gravity are the corrections up to it? *Exploration Geophysics*, 29, 378-383.

Fouillac, A. M., A. Dommanget, J. P. Milési. 1993. A carbon, oxygen, hydrogen and sulfur isotopic study of the gold mineralization at Loulo, Mali. *Chemical Geology* 106 (1-2): 47–62.

Gao, J., Yang, C., Ji, F., Wang, W., Shen, Z. 2017. Analyses on Origin of positive gravity anomalies of sedimentary basins of the Ross Sea. *EGU General Assembly Conference Abstracts*, 19, 17782. 2017 in Vienna, Austria.

Gueye, M., Ngom, P.M., Diène, M., Thiam, Y., Siegesmund, S., Wemmer, K., Pawlig, S. 2008. Intrusive rocks and tectono-metamorphic evolution of the Mako Paleoproterozoic belt (eastern Senegal, West Africa). *Journal of African Earth Sciences* 50 (2-4): 88–110.

Gueye, M., Siegesmund, S., Wemmer, K., Pawlig, S., Drobe, M., Nolte, N., Layer, P. 2007. New evidences for an early Birimian evolution in the West African Craton: An example from the Kedougou-Kenieba inlier, southeast Senegal. *South African Journal of Geology* 110 (4): 511–534.

Gunn, P. J. 1975. Linear transformations of gravity and magnetic fields. *Geophysical Prospecting*, 23 (2), 300-312. https://doi.org/10.1111/j.1365-2478.1975.tb01530.x

Gunn, P. J. 1997. Regional magnetic and gravity responses of extensional sedimentary basins. AGSO *Journal of Australian Geology and Geophysics*, 17(2), 115- 131.

Gunn, P. J., Maidment, D., and Milligan, P. R., 1997. Interpreting aeromagnetic data in areas of limited outcrop. AGSO *Journal of Australian Geology and Geophysics*, 17(2), 175-185.

Hansen, R. O. 2001. Gravity and magnetic methods at the turn of the millennium. *Geophysics* 66 (1): 36–37.

Hein, K.A.A., Matsheka, I.R., Bruguier, O., Masurel, Q., Bosch, D., Caby, R., Monié, P., 2015. The Yatela gold deposit: 2 billion years in the making. *Journal of African Earth Sciences* 112, 548–569.

Hirdes, W., and D. W. Davis. 2002. U–Pb geochronology of Paleoproterozoic rocks in the southern part of the Kedougou-Kenieba Inlier, Senegal, West Africa: evidence for diachronous accretionary development of the Eburnean province. *Precambrian Research* 118 (1-2): 83–99.

Holden, D.J., Nicholas J. Archibald, Fabio Boschetti, and Mark W. Jessell. 2000. Inferring geological structures using wavelet-based multiscale edge analysis and forward models. *Exploration geophysics* 31 (4): 617–621.

Hornby, P., F. Boschetti, and F. G. Horowitz. 1999. Analysis of potential field data in the wavelet domain. *Geophysical Journal International* 137 (1): 175–196.

Horowitz, F.G., Strykowski, G., Boschetti, F., Hornby, P., Archibald, N., Holden, D., Ketelaar, P., Woodcock, R. 2000. Earthworms;"multiscale" edges in the EGM96 global gravity field. In *SEG Technical Program Expanded Abstracts 2000*, 414–417. Society of Exploration Geophysicists.

Jacobsen, B.H., 1987. A case for upward continuation as a standard separation filter for potential-field maps. *Geophysics*. 52, 1138–1148.

Jessell, M., Santoul, J., Baratoux, L., Youbi, N., Ernst, R.E., Metelka, V., Miller, J., Perrouty, S. 2015. An updated map of West African mafic dykes. *Journal of African Earth Sciences* 112: 440–450.

Jessell, M.W., Begg, G.C., Miller, M.S. 2016. The geophysical signatures of the West African Craton. *Precambrian Research* 274: 3–24.

Kouamelan, A. N., Delor, C., Peucat, J. J. 1997. Geochronological evidence for reworking of Archean terrains during the early Proterozoic (2.1 Ga) in the western Cote d'Ivoire (Man Rise-West African Craton). *Precambrian Research*, 86(3), 177-199.

Karner, G. D.; Studinger, M.; Bell, R. 2005. Gravity anomalies of sedimentary basins and their mechanical implications: Application to the Ross Sea basins, West Antarctica. *Earth and Planetary Science Letters* 235(3):577-596. DOI: 10.1016/j.epsl.2005.04.016.

Kohanpour, F.; Lindsay, M. D.; Occhipinti, S.; Gorczyk, W. 2018. Structural controls on proterozoic nickel and gold mineral systems identified from geodynamic modelling and geophysical interpretation, east Kimberley, Western Australia. *Ore Geology Reviews* 95 (2018) 552–568. https://doi.org/10.1016/j.oregeorev.2018.03.010

Lambert-Smith, J.S., Lawrence, D.M, Müller, W., Treloar. P.J. 2016. Palaeotectonic setting of the south-eastern Kédougou-Kéniéba Inlier, West Africa: new insights from igneous trace element geochemistry and U-Pb zircon ages. *Precambrian Research* 274: 110–135.

Lambert-Smith, J.S., Lawrence, D.M, Vargas, C.A, Boyce, A.J., Treloar, P.J., Herbert, S. 2016. The Gounkoto Au deposit, West Africa: Constraints on ore genesis and volatile sources from petrological, fluid inclusion and stable isotope data. *Ore Geology Reviews* 78: 606–622.

Lambert-Smith, J.S., Rocholl, A., Treloar, P.J., Lawrence, D.M. 2016. Discriminating fluid source regions in orogenic gold deposits using B-isotopes. *Geochimica et Cosmochimica Acta* 194: 57–76.

Lawrence, D.M., Treloar, P.J., Rankin, A.H., Boyce, A., Harbidge, P. 2013b. A fluid inclusion and stable isotope study at the Loulo mining district, Mali, West Africa: Implications for multifluid sources in the generation of orogenic gold deposits. *Economic Geology* 108 (2): 229–257.

Lawrence, D.M., Treloar, P.J., Rankin, A.H., Harbidge, P., Holliday, J. 2013a. The geology and mineralogy of the Loulo mining district, Mali, West Africa: Evidence for two distinct styles of orogenic gold mineralization. *Economic Geology* 108 (2): 199–227.

Ledru, P., J. Pons, J. P. Milési, J. L. Feybesse, and V. Johan. 1991. Transcurrent tectonics and polycyclic evolution in the Lower Proterozoic of Senegal-Mali. *Precambrian Research* 50 (3-4): 337–354.

Leu, L.K. 1982. Use of reduction-to-the-equator process for magnetic data interpretation. In *Geophysics*, 47:445–445. Society Exploration Geophysicists 8801 syalest, tulsa, 74137.

Lyngsie, S.B., Thybo, H., Rasmussen, T.M., 2006. Regional geological and tectonic structures of the North Sea area from potential field modelling. *Tectonophysics* 413, 147–170.

MacLeod, I.N., Jones, K., Dai, T.F. 1993. 3-D analytic signal in the interpretation of total magnetic field data at low magnetic latitudes. *Exploration Geophysics* 24 (4): 679–

688.

Masurel, Q., Thébaud, N., Miller, J., Ulrich, S. 2017c. The tectono-magmatic framework to gold mineralisation in the Sadiola-Yatela gold camp and implications for the paleotectonic setting of the Kédougou-Kénieba inlier, West Africa. *Precambrian Research* 292: 35–56.

Masurel, Q., Thébaud, N., Miller, J., Ulrich, S., Hein, K.A.A., Cameron, G., Béziat, D., Bruguier, O., Davis, J.A. 2017a. Sadiola Hill: A world-class carbonate-hosted gold deposit in Mali, West Africa. *Economic Geology* 112 (1): 23–47.

Masurel, Q., Thébaud, N., Miller, J., Ulrich, S., Roberts, M.P., Béziat, D. 2017b. The Alamoutala Carbonate-Hosted Gold Deposit, Kédougou-Kénieba Inlier, West Africa. *Economic Geology* 112 (1): 49–72.

McCuaig, T.C., and Kerrich, R. 1998. P—T—t—deformation—fluid characteristics of lode gold deposits: evidence from alteration systematics. *Ore Geology Reviews* 12 (6): 381–453.

Milési, J.P., Ledru, P., Feybesse, J.L., Dommanget, A., Marcoux, E. 1992. Early Proterozoic ore deposits and tectonics of the Birimian orogenic belt, West Africa. *Precambrian Research* 58 (1-4): 305–344.

Miller, H.G. and Singh, V., 1994. Potential field tilt – a new concept for location of potential field sources. *Journal of Applied Geophysics* 32, 213–217.

Milligan, P. R., and P. J. Gunn. 1997. Enhancement and presentation of airborne geophysical data. *AGSO Journal of Australian Geology and Geophysics* 17 (2): 63–75.

Nabighian, M.N., Grauch, V. J. S., Hansen, R. O., LaFehr, T. R., Li, Y., Peirce, J. W., Phillips, J. D., Ruder, M. E. 2005. The historical development of the magnetic method in exploration. *Geophysics* 70 (6): 33ND–61ND.

Ndiaye, P. M., Dia, A., Vialette, Y., Diallo, D. P., Ngom, P. M., Sylla, M., Wade, S., Dioh, E. 1997. Données pétrographiques, geochimiques et géochronologiques nouvelles sur les granitoïdes du Paléoprotérozoïque du Supergroupe de Dialé-Daléma (Sen; égal Oriental): Implications pétrogénétiques et géodynamiques. *Journal of African Earth Sciences* 25 (2): 193–208.

Ngom, P. M., Rocci, G., Debat, P., Dia, A., Diallo, D. P., Dioh, E., Sylla, M. 1997. Les massifs basiques et ultrabasiques birimiens du supergroupe de Mako (Sénégal oriental): pétrographie, géochimie et signification pétrogénétique. *Bull. Ifan* 49: 33–54.

Ngom P.M., Teixeira W. Cordani U.G., 2009. Sr et Nd isotopic geochemistry of the early ultramafic-mafic rocks of the Mako bimodal volcanic belt of the Kedougou-Kenieba inlier (Senegal). *Arab J. Geoscience*. 3, 49-57.

Pons, J., Oudin, C., Valero, J. 1992. Kinematics of large syn-orogenic intrusions: example of the Lower Proterozoic Saraya batholith (Eastern Senegal). *Geologische Rundschau* 81

(2): 473–486.

Priestley, K., McKenzie, D., Debayle, E., Pilidou, S., 2008. The African upper mantle and its relationship to tectonics and surface geology. *Geophysics Journal International*. 175, 1108–1126

Ranganai, R. T., Whaler, K. A., Ebinger, C. J. 2008. Gravity anomaly patterns in the south-central Zimbabwe Archaean craton and their geological interpretation. *Journal of African Earth Sciences* 51 (5): 257–276.

Roest, W.R., Verhoef, J., Pilkington, M., 1992. Magnetic interpretation using the 3-D analytic signal. Geophysics 57, 116–125.

Sysmin, 2006. Projet de cartographie du Birimien malien. BRGM/RC-54684-FR, 356p.

Théveniaut, H., Ndiaye, P.M., Buscail, F., Couëffé, R., Delor, C., Fullgraf, T., Goujou, J.-C., 2010. Notice explicative de la carte géologique du Sénégal oriental à 1/500 000. Ministère des Mines, de l'Industrie, de l'Agro-Industrie et des PME, Direction des Mines et de la Géologie, Dakar.

Trompette, R. 1973. « Le Précambrien supérieur et le Paléozoïque inférieur de l'Adrar de Mauritanie (bordure occidentale du bassin de Taoudeni, Afrique de l'Ouest), un exemple de sédimentation de craton. Étude stratigraphique et sédimentologique- TOME 2 (Séries 2 et 3) ». *PhD Thesis*, Université de Provence-Aix-Marseille I.

Verduzco, B., Fairhead, J.D., Green, C.M., MacKenzie, C. 2004. New insights into magnetic derivatives for structural mapping. *The Leading Edge* 23 (2): 116–119.

Villeneuve, M., Bonvalot, S., Albouy, Y. 1990. L'agencement des chaînes (Panafricaines et Hercynienne) de la bordure occidentale du craton ouest africain. *Comptes Rendus de l'Académie des Sciences* 310: 955–959.

Villeneuve, M., 2008. Review of the orogenic belts on the western side of the West African Craton: the Bassarides, Rokelides and Mauritanides. In: Ennih, N., Liégeois, J.P. (Eds.), The Boundaries of the West African Craton, vol. 297, *Geological Society of London* Special Publication, 169–201.

Figure Captions

Figure 1: (a) - Geologic map of the West African craton (modified after Masurel et al., 2017c; Boher et al., 1992). (b) - Geologic map of the Kédougou-Kéniéba inlier (1:250,000 scale, modified after Gueye et al., 2007; Lawrence et al., 2013a). The Falémé River forms the international border with Senegal to the west and Mali to the east and north. *Abbreviation: KKI* = Kédougou-Kéniéba Inlier; *KMD* = Kénéma-Man Domain; *BMD* = Baoulé-Mossi Domain; Sa = Saraya Pluton; Yt = Yatea Pluton; Ga = Gamaye Pluton.

Figure 2: (a): Previously existing litho-structural map covering the gravity data (modified after Villeneuve, 2008). (b): The gravity data distribution (grey dots) and the resulting complete grid. The heavy dashed lines indicate structural interpretation while fine lines indicate main lithological domains inferred from (a). Abbreviation: MbT = Mauritanide Belt Thrust; BKKF = Bissau–Kidira–Kayes Fault Zone; KI = Kayes Inlier; KKI = Kédougou-Kéniéba Inlier; KM = Kénéma-Man domain.

Figure 3: (a): Bouguer gravity map before applying terrain correction. (b): Local-scale topographic data used in the calculation of the terrain correction. (c): Complete Bouguer map after applying the terrain correction.

Figure 4: Bouguer gravity maps and lineament interpretations. (a) to (c): Most prominent gravity lineaments interpreted from gravity data and superposed upon a- complete Bouguer gravity grid; b- its first vertical derivative and c- its upward continued map at 20 km depth; (d) Structural interpreted map from gravity on geological map in Fig.2a. Known structures modified from Villeneuve, (2008) are represented in black lines and new structural interpretation are represented in blue dashed lines. Abbreviation: KSZ: Kayes Shear Zone; KKSZ: Kédougou-Kéniéba Shear Zone; SSZ: South Shear Zone; NCSZ = North Crustal Shear Zone; SCSZ = North Crustal Shear Zone

Figure 5: Upward continuation gravity worms (rainbow coloured lines) from ~7 km upward continuation in green to ~57 km upward continuation in red with (a) on the greyscale

complete Bouguer gravity map with interpreted gravity lineaments in Fig. 3 and gold deposits in the region; (b) on the litho-tectonic map from Villeneuve, (2008) and gold deposited in the region. Distribution of gold deposits in the gravity worm image shows that gold deposits are located in or near lower-order structures. Acronyms 1 to 10 are referred to geological features discussed in the text.

Figure 6: Presentation of magnetic data. (a) - Image of the reduced to equator total magnetic intensity; (b): Image of the first vertical derivative of the RTE magnetic field (c) Image of the analytic signal of the RTE magnetic field. (d) Tilt derivative of the RTE aeromagnetic map.

Figure 7: (a) Image of the analytic signal of the RTE magnetic field with abbreviations of units/features; (b) Lithological interpretation defined from the analytic signal map and based on the definition of magnetic responses. The different families of color are magnetically distinct subdivisions of the inlier in two part; (c): Zoom of KKI zone with structural interpretation from first vertical derivative gravity data. Abbreviation: A to L = Acronyms of magnetic and gravity anomalies; MTZ = Main Transcurrent Zone; SMSZ = Senegal-Malian Shear Zone; KKSZ = Kédougou-Kéniéba Shear Zone; NCSZ = North Crustal Shear Zone; Ga = Gamaye monzogranite; Sa = Saraya granitoids; Yt = Yatea monzogranite; Mo = Moussala granodiorite; Ta: Mesoproterozoic to Paleozoic Taoudeni basin; Sd: Doleritic sill intrusion.

Figure 8: (a): Most prominent magnetic lineaments from and superposed upon a greyscale image of the first vertical derivative of the RTE magnetic field and lineament interpretations with lineaments inferred from gravity. (b): Magnetic lineaments interpreted from the enhanced first vertical derivative of the RTE magnetic field superposed on upward continued magnetic data at 2.5 km depth.

Figure 9: (a): Image of the tilt derivative of the RTE magnetic field. (b): Magnetic lineaments associated to dolerite dykes interpreted from the tilt derivative map and rose diagram of dyke orientations.

Figure 10: Simplified geological map of the Malian part of the KKI and surrounding rocks of the Taoudeni basin displaying key lithological units and structural framework interpreted from gravity and magnetic data.

Table captions

Table 1: Zoom on deep shears and thrusts interpreted in the studied area and their regional-scale gravity response. Abbreviation: 1VD = First vertical derivative; BA = Bouguer anomaly; Upward Cnt = Upward continuation.

Table 2: Key parameters of geophysical data sets from Mali

Table 3: Zoom on near-surface faults and shear zones interpreted in the Malian part of the KKI and their local-scale magnetic response. Abbreviation: RTE = Reduced to Equator; 1VD = First vertical derivative.

FIG1:

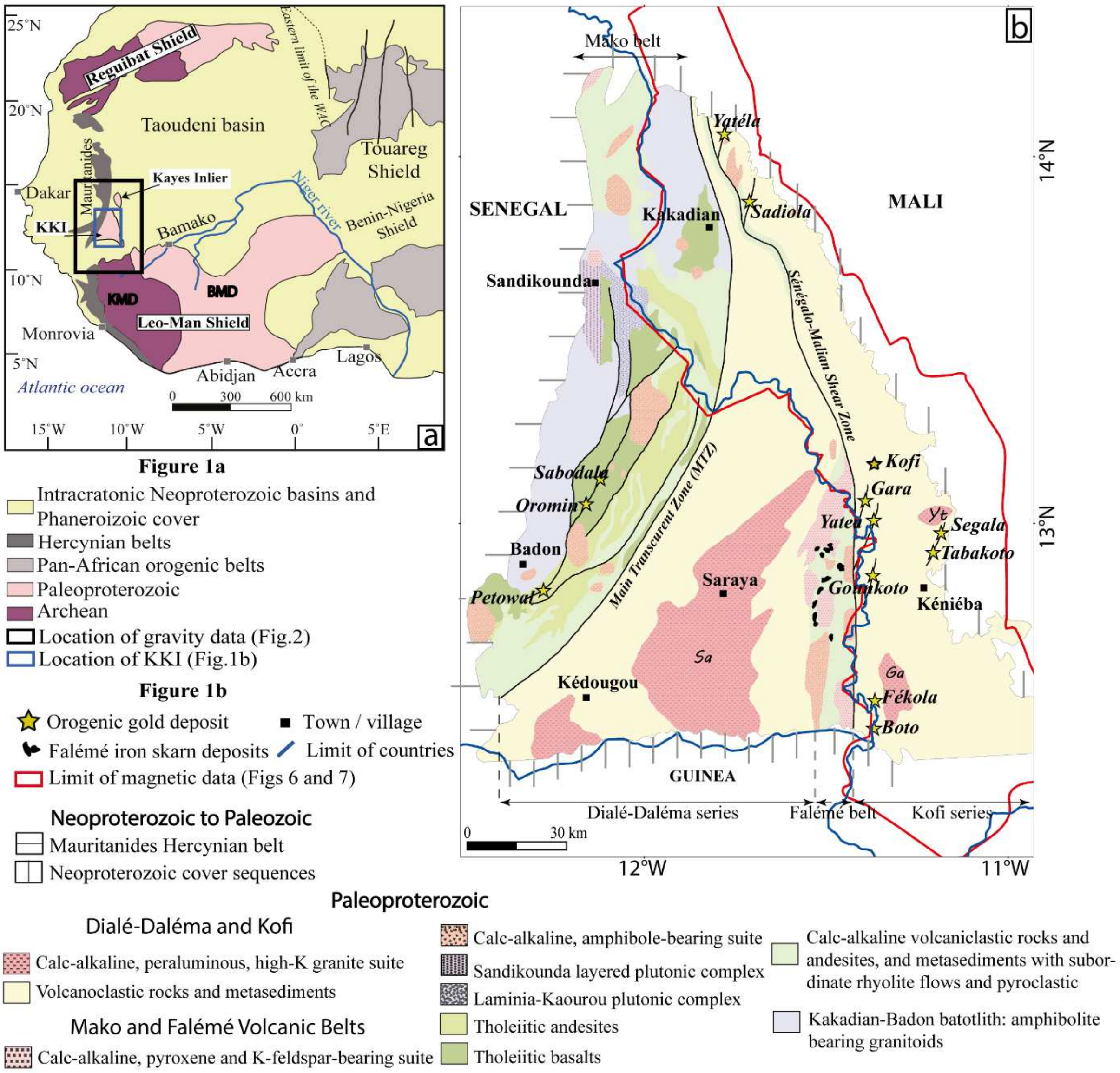

Reguibat Shield
Taoudeni basin
Eastern limit of the WAC
Touareg Shield
Kayes Inlier
Mauritanides
Dakar
KKI
Bamako
Niger river
Benin-Nigeria Shield
KMD
BMD
Leo-Man Shield
Monrovia
Abidjan
Accra
Lagos
Atlantic ocean
25°N
20°N
10°N
5°N
15°W
10°W
5°W
0°
5°E
0 300 600 km
a
b
Mako belt
SENEGAL
MALI
GUINEA
Yatéla
Sadiola
Kakadian
Sandikounda
Sénégalo-Malian Shear Zone
Main Transcurent Zone (MTZ)
Sabodala
Oromin
Badon
Petowal
Saraya
Kédougou
Sa
Kofi
Gara
Yatea
Yt
Segala
Tabakoto
Gounkoto
Kéniéba
Ga
Fékola
Boto
Dialé-Daléma series
Falémé belt
Kofi series
0 30 km
12°W
11°W
14°N
13°N
Figure 1a
Intracratonic Neoproterozoic basins and Phaneroizoic cover
Hercynian belts
Pan-African orogenic belts
Paleoproterozoic
Archean
Location of gravity data (Fig.2)
Location of KKI (Fig.1b)
Figure 1b
Orogenic gold deposit
Town / village
Falémé iron skarn deposits
Limit of countries
Limit of magnetic data (Figs 6 and 7)
Neoproterozoic to Paleozoic
Mauritanides Hercynian belt
Neoproterozoic cover sequences
Paleoproterozoic
Dialé-Daléma and Kofi
Calc-alkaline, peraluminous, high-K granite suite
Volcanoclastic rocks and metasediments
Mako and Falémé Volcanic Belts
Calc-alkaline, pyroxene and K-feldspar-bearing suite
Calc-alkaline, amphibole-bearing suite
Sandikounda layered plutonic complex
Laminia-Kaourou plutonic complex
Tholeiitic andesites
Tholeiitic basalts
Calc-alkaline volcaniclastic rocks and andesites, and metasediments with subordinate rhyolite flows and pyroclastic
Kakadian-Badon batotlith: amphibolite bearing granitoids

FIG2:

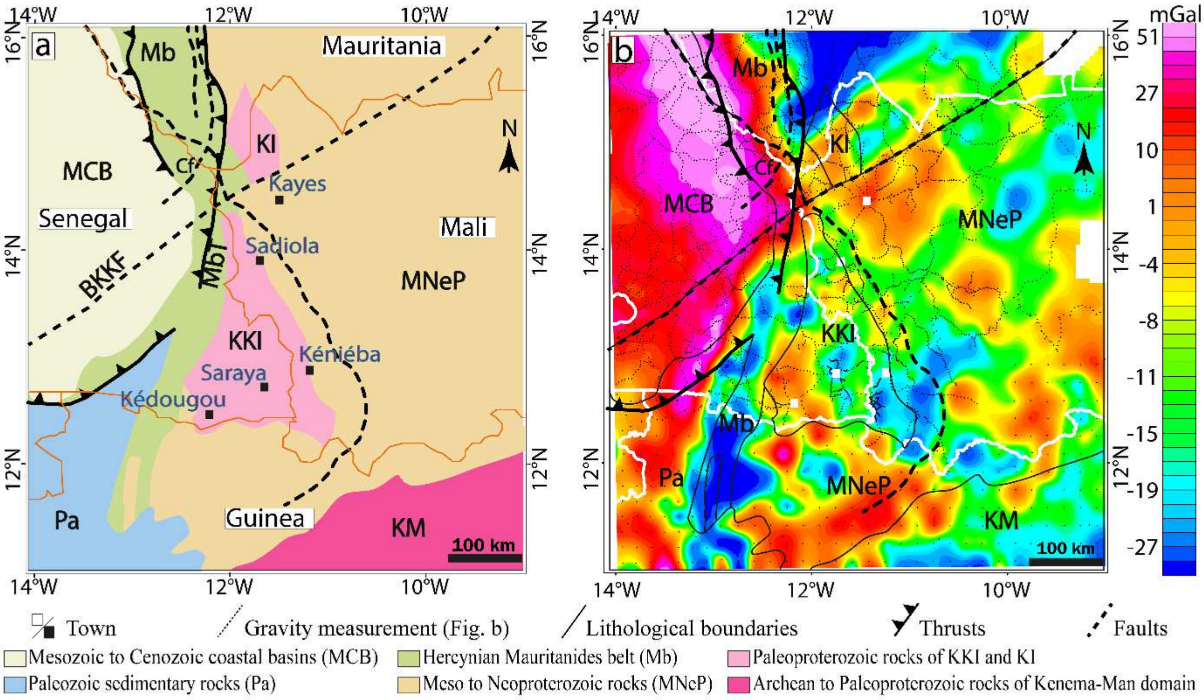
a
b
Mb
Mauritania
KI
MCB
Cf
Kayes
Senegal
Mali
Sadiola
MNeP
BKKF
Mbt
KKI
Kéniéba
Saraya
Kédougou
Pa
Guinea
KM
100 km
N
14°W
12°W
10°W
16°N
14°N
12°N
mGal
51
27
10
1
-4
-8
-11
-15
-19
-27
Town
Gravity measurement (Fig. b)
Lithological boundaries
Thrusts
Faults
Mesozoic to Cenozoic coastal basins (MCB)
Hercynian Mauritanides belt (Mb)
Paleoproterozoic rocks of KKI and KI
Paleozoic sedimentary rocks (Pa)
Meso to Neoproterozoic rocks (MNeP)
Archean to Paleoproterozoic rocks of Kenema-Man domain

FIG3:

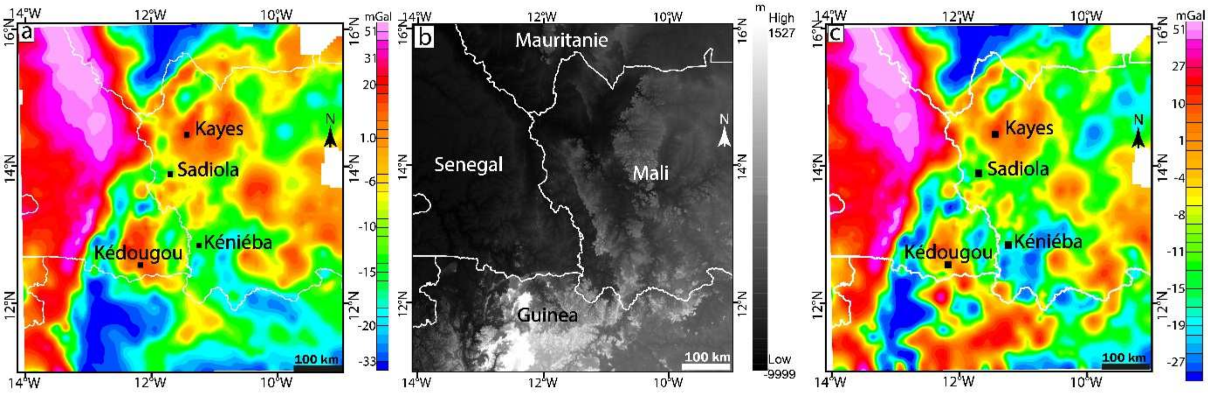

a
Kayes
Sadiola
Kédougou
Kéniéba
mGal
100 km
N
b
Mauritanie
Senegal
Mali
Guinea
m
High
1527
Low
-9999
100 km
N
c
Kayes
Sadiola
Kédougou
Kéniéba
mGal
100 km
N

FIG4:

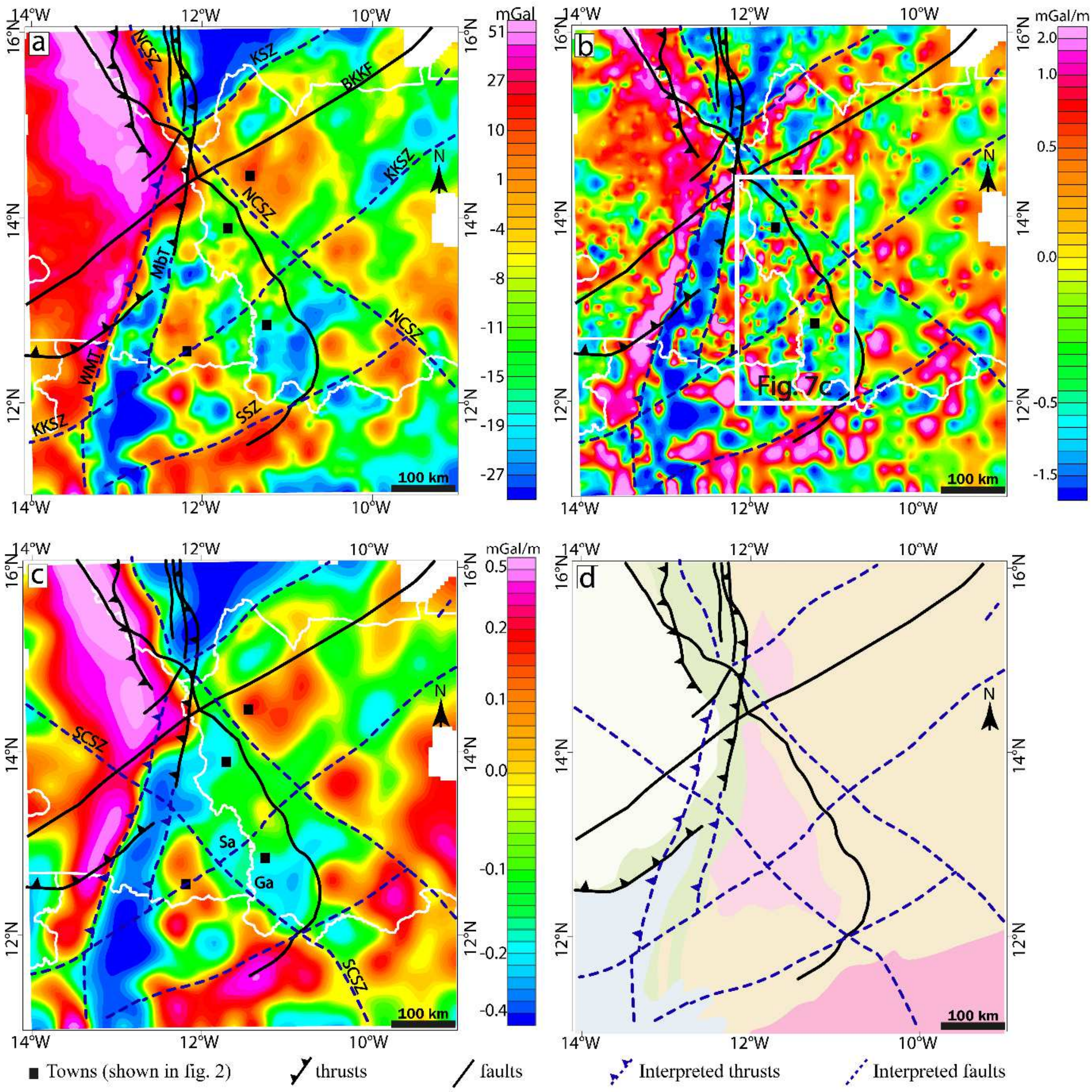

a
b
c
d
14°W
12°W
10°W
16°N
14°N
12°N
mGal
51
27
10
1
-4
-8
-11
-15
-19
-27
mGal/m
2.0
1.0
0.5
0.0
-0.5
-1.5
0.2
0.1
-0.1
-0.2
-0.4
NCSZ
KSZ
BKKF
KKSZ
MbT
WMT
SSZ
SCSZ
Sa
Ga
Fig. 7c
N
100 km
Towns (shown in fig. 2)
thrusts
faults
Interpreted thrusts
Interpreted faults

FIG5:

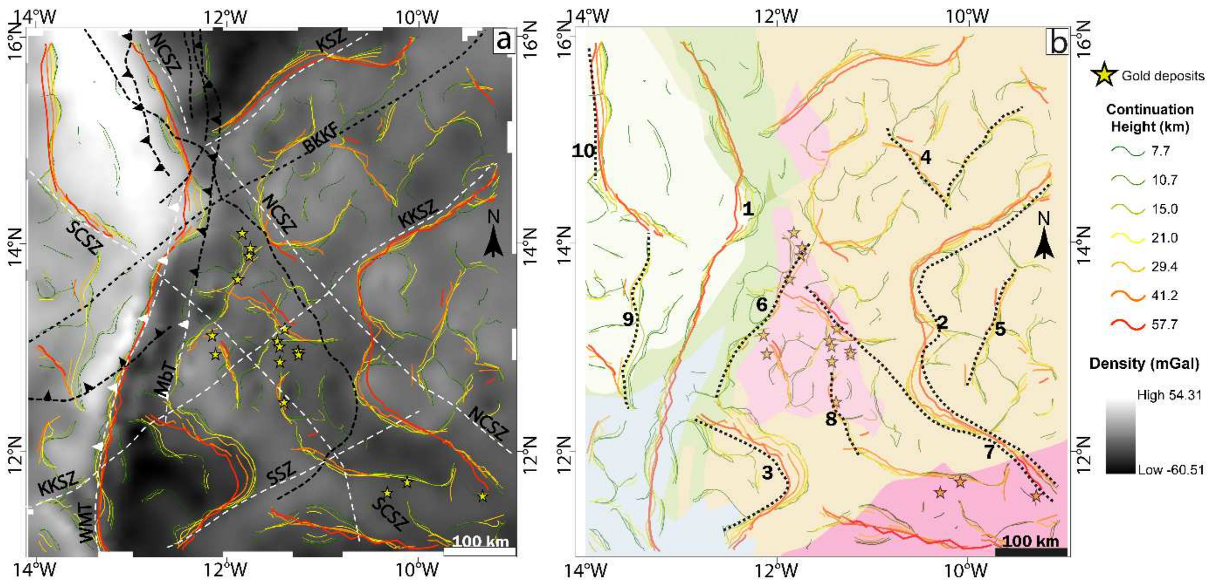

a
b
14°W
12°W
10°W
16°N
14°N
12°N
N
100 km
NCSZ
KSZ
BKKF
SCSZ
KKSZ
MbT
SSZ
WMT
1
2
3
4
5
6
7
8
9
10
Gold deposits
Continuation Height (km)
7.7
10.7
15.0
21.0
29.4
41.2
57.7
Density (mGal)
High 54.31
Low -60.51

FIG6:

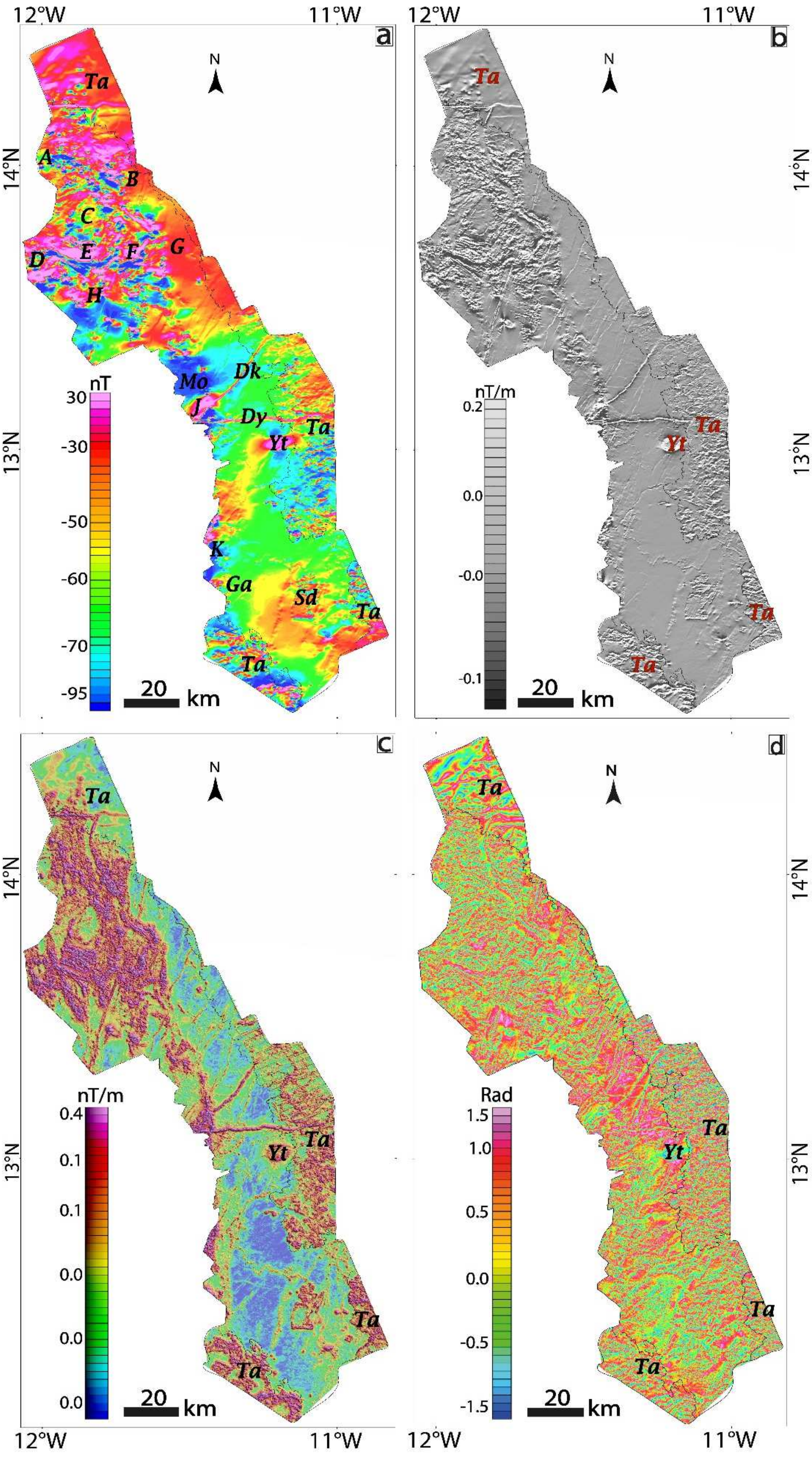
12°W
11°W
14°N
13°N
N
a
b
c
d
Ta
A
B
C
D
E
F
G
H
Mo
Dk
J
Dy
Yt
K
Ga
Sd
nT
30
-30
-50
-60
-70
-95
nT/m
0.2
0.0
-0.0
-0.1
0.4
0.1
Rad
1.5
1.0
0.5
-0.5
-1.5
20 km

FIG7:

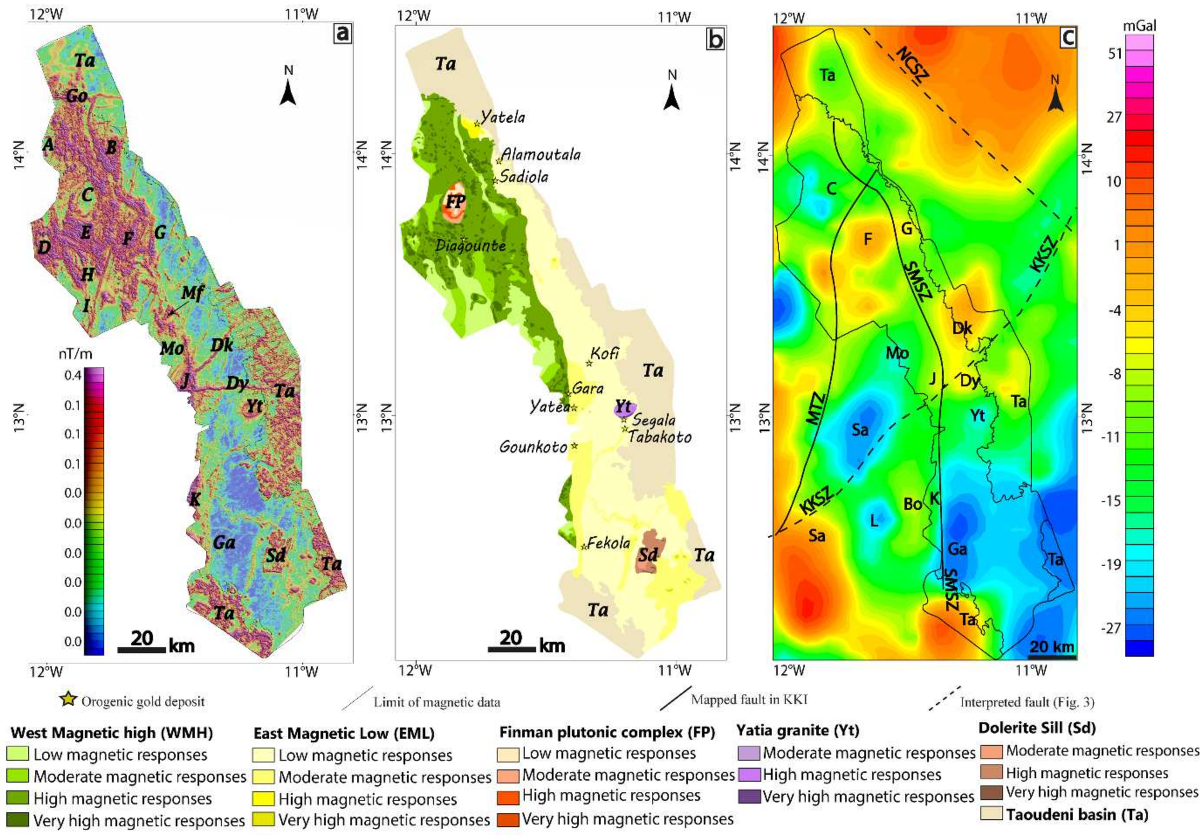

a
b
c
12°W
11°W
14°N
13°N
N
nT/m
mGal
20 km
Ta
Go
A
B
C
D
E
F
G
H
I
Mf
Mo
Dk
J
Dy
Yt
K
Ga
Sd
FP
Yatela
Alamoutala
Sadiola
Diagounte
Kofi
Gara
Yatea
Segala
Tabakoto
Gounkoto
Fekola
NCSZ
SMSZ
KKSZ
MTZ
Sa
L
Bo
Orogenic gold deposit
Limit of magnetic data
Mapped fault in KKI
Interpreted fault (Fig. 3)
West Magnetic high (WMH)
Low magnetic responses
Moderate magnetic responses
High magnetic responses
Very high magnetic responses
East Magnetic Low (EML)
Low magnetic responses
Moderate magnetic responses
High magnetic responses
Very high magnetic responses
Finman plutonic complex (FP)
Low magnetic responses
Moderate magnetic responses
High magnetic responses
Very high magnetic responses
Yatia granite (Yt)
Moderate magnetic responses
High magnetic responses
Very high magnetic responses
Dolerite Sill (Sd)
Moderate magnetic responses
High magnetic responses
Very high magnetic responses
Taoudeni basin (Ta)

FIG8:

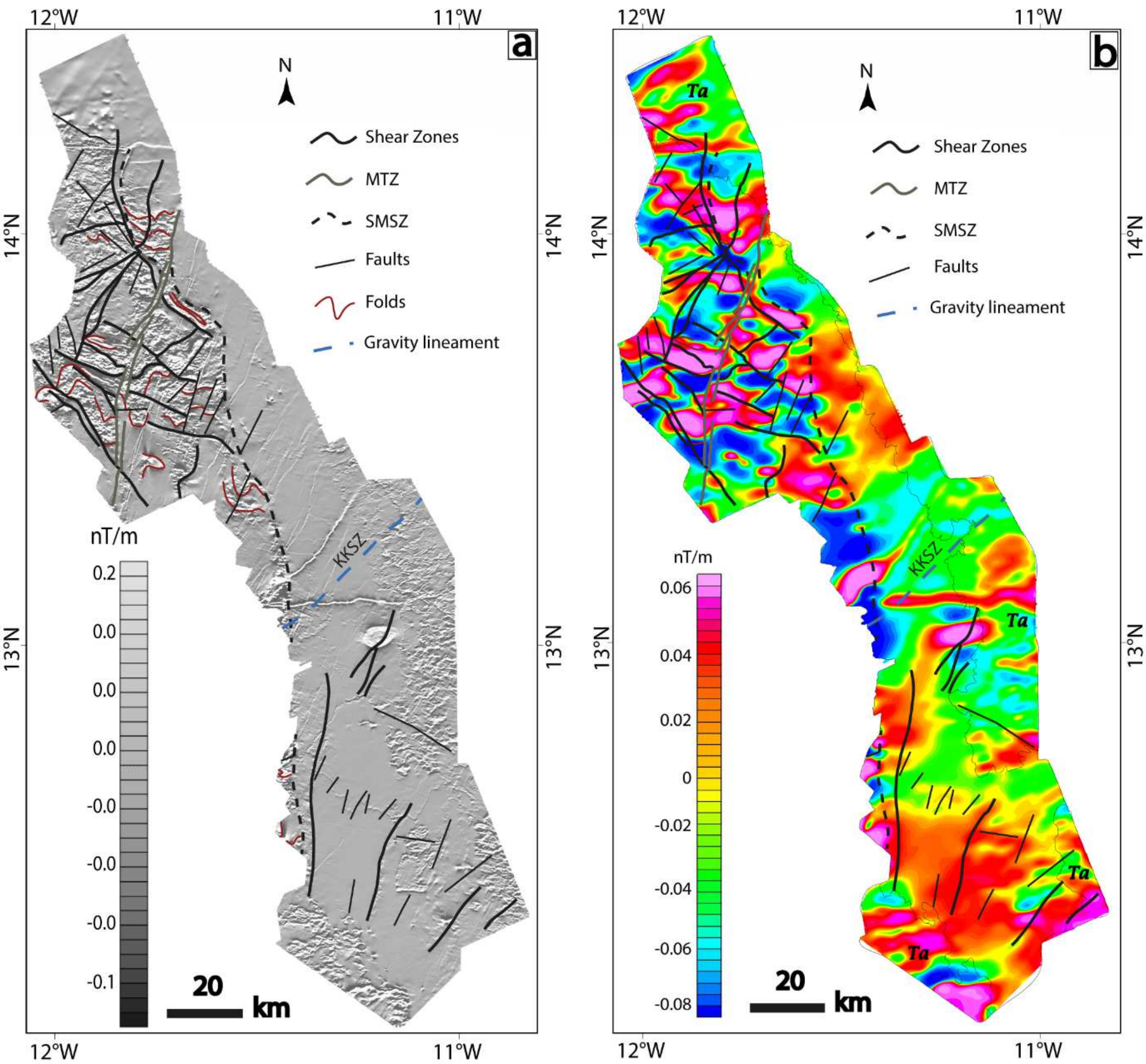
12°W
11°W
14°N
13°N
a
b
N
Shear Zones
MTZ
SMSZ
Faults
Folds
Gravity lineament
KKSZ
nT/m
0.2
0.0
-0.0
-0.1
20
km
Ta
0.06
0.04
0.02
0
-0.02
-0.04
-0.06
-0.08

FIG9:

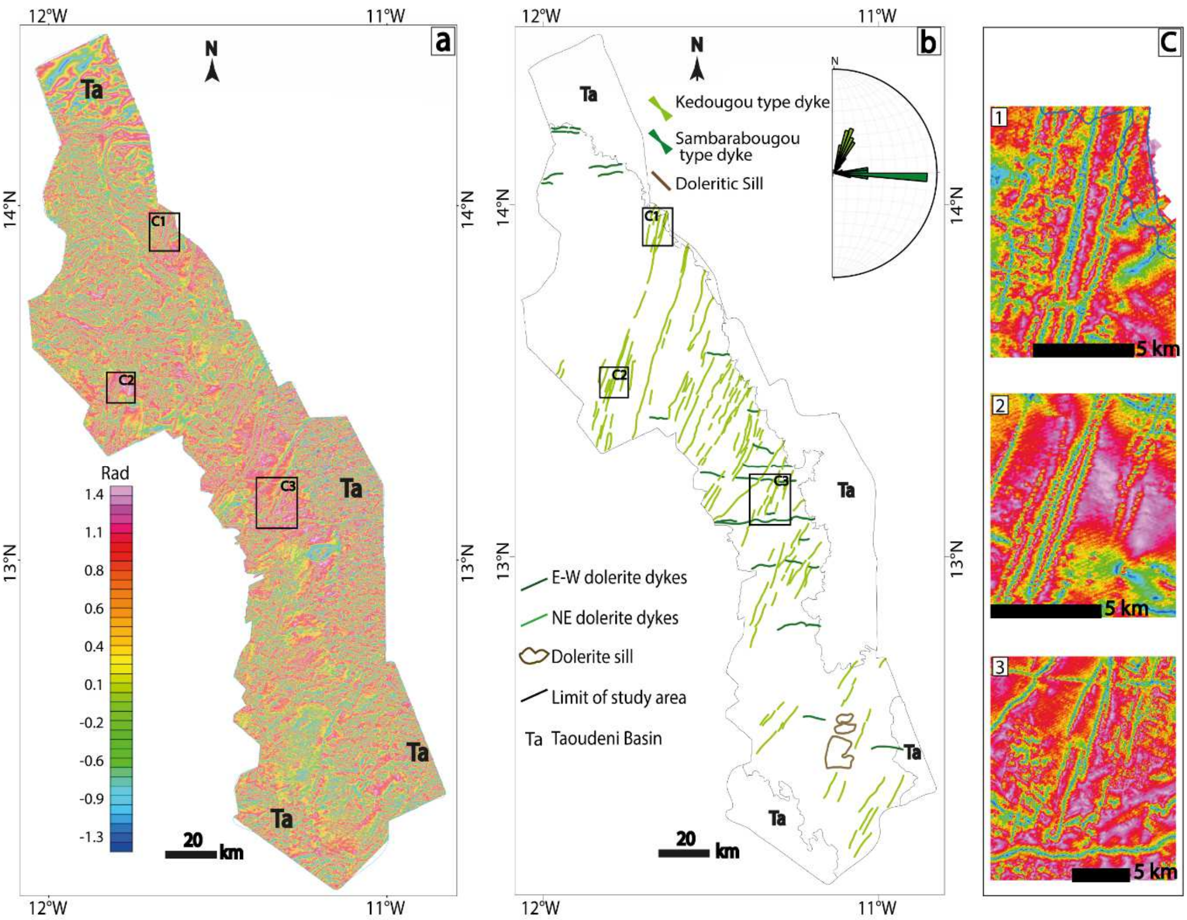

a
b
C
12°W
11°W
14°N
13°N
N
Ta
C1
C2
C3
Rad
1.4
1.1
0.8
0.6
0.4
0.1
-0.2
-0.6
-0.9
-1.3
20 km
Kedougou type dyke
Sambarabougou type dyke
Doleritic Sill
E-W dolerite dykes
NE dolerite dykes
Dolerite sill
Limit of study area
Ta Taoudeni Basin
1
2
3
5 km

FIG10:

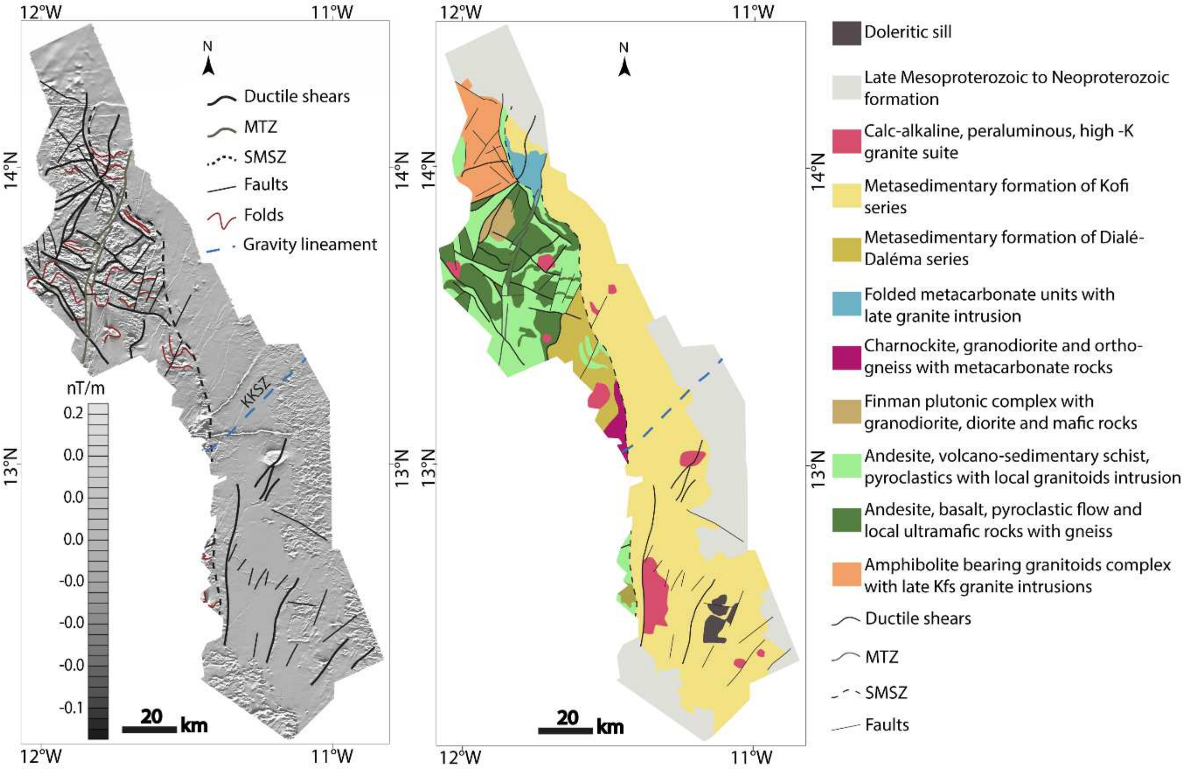

12°W
11°W
14°N
13°N
N
Ductile shears
MTZ
SMSZ
Faults
Folds
Gravity lineament
KKSZ
nT/m
0.2
0.0
0.0
0.0
-0.0
-0.0
-0.0
-0.1
20 km
Doleritic sill
Late Mesoproterozoic to Neoproterozoic formation
Calc-alkaline, peraluminous, high -K granite suite
Metasedimentary formation of Kofi series
Metasedimentary formation of Dialé-Daléma series
Folded metacarbonate units with late granite intrusion
Charnockite, granodiorite and ortho-gneiss with metacarbonate rocks
Finman plutonic complex with granodiorite, diorite and mafic rocks
Andesite, volcano-sedimentary schist, pyroclastics with local granitoids intrusion
Andesite, basalt, pyroclastic flow and local ultramafic rocks with gneiss
Amphibolite bearing granitoids complex with late Kfs granite intrusions
Ductile shears
MTZ
SMSZ
Faults

Table 1:

Structure	Name	Sense	Gravity characteristics	Map gravity responses	Images on
Deep unexposed faults from complete Bouguer anomaly map and its first vertical derivative analyses	MTZ and WMT	Undefined	Apparent alignment of gravity anomalies/contacts defined as borders of gravity anomalies; gravity lineaments along offset of gravity anomalies; and gravity lineaments from offset of density or juxtaposition of contrasted gravity domains	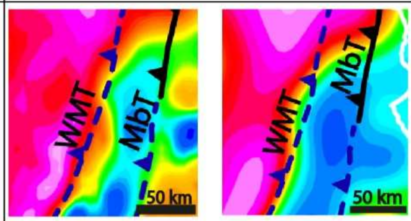	BA and Upward Cnt
	KSZ	Undefined		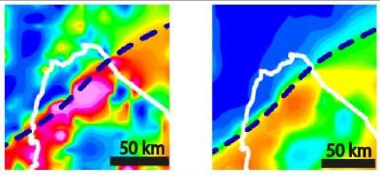	1VD and BA
	KKSZ	Dextral		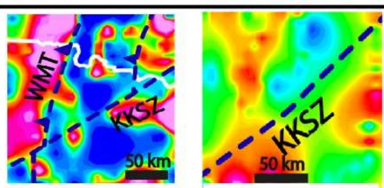	1VD
	SSZ	Sinistral		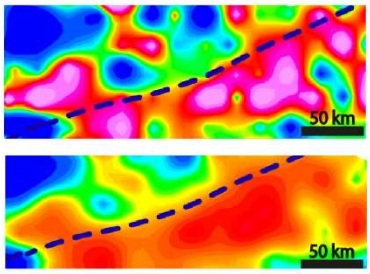	1VD and BA
	NCSZ	Undefined		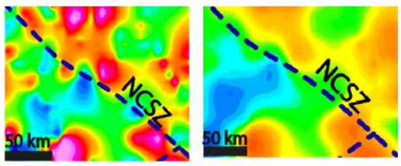	1VD and BA
	SCSZ	Undefined		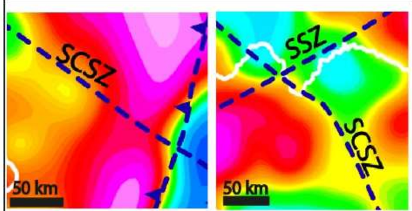	Upward Cnt

Table 2:

	High - Sense	*Kevron*
Survey area	Kéniéba	Kéniéba
Survey period	1996 and 1997	2001
Acquisition company	High – Sense Geophysics Ltd	Kevron Pty Ltd
Survey type	Combined airborne	Combined airborne
Altitude	100 m	100 m
Flight orientation	000 – 180° and 065 – 245°	000 – 180° and 065 – 245°
Line spacing	200 m	200 m
Tie line orientation	065 – 245° and 155 – 335°	065 – 245° and 155 – 335°
Tie line spacing	3000 m	3000 m
Time interval in recording	0.1 s	0.1 s

Table 3:

Structure	Name	Sense	Magnetic characteristics	Corresponded images	Images on
Near-surface structural framework from the RTE and its first vertical derivative maps	SMSZ	Undefined	Abrupt magnetic contact between contrasting magnetic domains	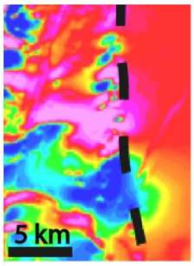 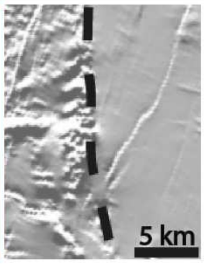	RTE and 1VD
	MTZ	Sinistral and Dextral	Slightly curved discontinuity that cuts (locally offset) magnetic units	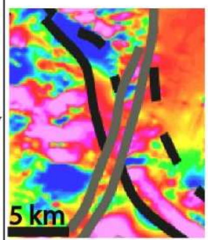 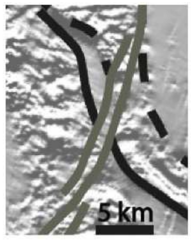	RTE and 1VD
	Folds	Sinistral (fault)	Folded magnetic horizons with fault/shear in axial plane	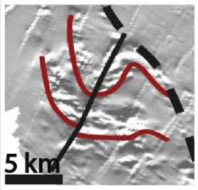 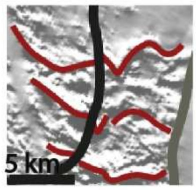	1VD
	Faults in Mako belt	Sinistral and Dextral	Straight discontinuities that cut and offset high magnetic units	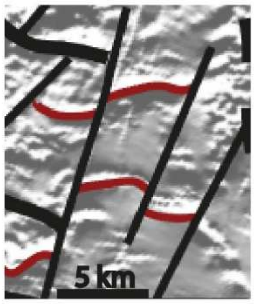	1VD
	Faults in Kofi series	Dextral			1VD
	Faults in mafic sill	Sinistral		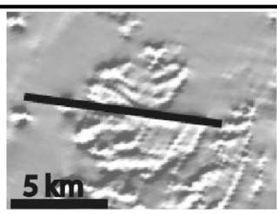	1VD